Photolytic Hazes in the Atmosphere of 51 Eri b

K. Zahnle

NASA Ames Research Center, Moffett Field, CA 94035

Kevin.J.Zahnle@NASA.gov

M. S. Marley

NASA Ames Research Center, Moffett Field, CA 94035

Mark.S.Marley@NASA.gov

and

C. V. Morley

Department of Astronomy and Astrophysics, University of California, Santa Cruz, CA 95064

cmorley@ucolick.org

and

J. I. Moses

Space Science Institute, 4750 Walnut Street, Suite 205, Boulder, CO 80301

jmoses@spacescience.org

ABSTRACT

We use a 1D model to address photochemistry and possible haze formation in the irradiated warm Jupiter 51 Eridani b. The intended focus was to be carbon, but sulfur photochemistry turns out to be important. The case for organic photochemical hazes is intriguing but falls short of being compelling. If they form, they are likeliest to do so if vertical mixing in 51 Eri b is weaker than in Jupiter, and they would be found below the regions where methane and water are photolyzed. The more novel result is that photochemistry turns H_2S into elemental sulfur, here treated as S_8. In the cooler models, S_8 is predicted to condense in optically thick clouds of solid sulfur particles, whilst in the warmer models S_8 remains a vapor along with several other sulfur allotropes that are both visually striking and potentially observable. For 51 Eri b, the division between models with and without condensed sulfur is at an effective temperature of

700 K, which is within error its actual effective temperature; the local temperature where sulfur condenses is between 280 and 320 K. The sulfur photochemistry we have discussed is quite general and ought to be found in a wide variety of worlds over a broad temperature range, both colder and hotter than the 650-750 K range studied here, and we show that products of sulfur photochemistry will be nearly as abundant on planets where the UV irradiation is orders of magnitude weaker than it is on 51 Eri b.

Subject headings: planetary systems — stars: individual(51 Eri b)

1. Introduction

The star 51 Eridani is a pre-main-sequence F dwarf that is only 20 million years old. Direct-imaging observations with GPI (Gemini Planet Imager) reveal that the star is orbited by a self-radiant young Jupiter, designated 51 Eri b, that emits with an effective temperature on the order of $T_{\rm eff} = 700 \pm 50$ K (Macintosh et al. 2015). Thermal evolution models predict that a 20 Myr old jovian planet with 51 Eri b's luminosity will have mass $\sim 2M_{\rm Jup}$ and radius $\sim 1R_{\rm Jup}$ (Macintosh et al. 2015).

Comparison by Macintosh et al. (2015) of the available spectral and photometric data to spectral models reveal that while the planet shows methane in absorption, methane is depleted compared to thermochemical equilibrium. Carbon monoxide is therefore expected to be abundant but available data do not yet constrain it. Spectral matching with radiative transfer models also strongly suggest that clouds, possibly patchy, are present in the atmosphere (Macintosh et al. 2015). However, the planet is cool enough that silicate clouds if present would be confined to levels deep beneath the photosphere and thus unlikely to affect what can be seen. Clouds of salts like Na_2S and NaCl are possible, but even these would be expected to be confined to levels beneath the photosphere by the low temperature of the planet (Morley et al. 2012).

In this study we use a 1D chemical kinetics model to ask whether, and under what conditions, photochemical hazes are likely to form in the atmosphere of 51 Eri b and perhaps be the agent responsible for the observed particulate opacity. We consider two candidates, one familiar, the other more novel. The familiar candidate is an organic photochemical haze loosely analogous to the hazes seen over Titan, Pluto, or Beijing. Such hazes have been proposed by many workers, but to date the case for them has been inconclusive (Moses 2014). We will find here that a reasonable case for a photochemical organic haze in 51 Eri b can be made, but we do not follow the chain of polymerization reactions to molecules big enough and refractory enough that we can prove that condensates actually form. The novel candidate is sulfur. With sulfur we can follow a much shorter chain of polymerization to the point where sulfur condenses. We will show here that a good case can be made for the presence of photochemical sulfur clouds in the atmosphere of 51 Eri b.

This paper begins with a brief review of some related previous work. We next reprise our own

model. In section 4 we present results for models that span the parameter space in which 51 Eri b probably resides. We will find that for some of these parameters organic hazes might form, and for some parameters sulfur clouds will form, for some parameters both might form, and for some parameters neither kind of haze is likely to form. The important role of sulfur raises the issue that much of the sulfur chemistry is very poorly known. In section 5 we perform a series of sensitivity tests to examine how the model responds to alternative assumptions about sulfur's photochemistry.

2. Previous Models

The possibility that photochemical organic hazes might be important in irradiated brown dwarfs was first raised by Griffith et al. (1998). It remains an open question.

The first exoplanet photochemical models showed that small hydrocarbons would not condense in the solar composition atmospheres of hot Jupiters (Liang et al. 2003, 2004). Line et al. (2010, 2011) confirmed this result for hot Jupiters. They predicted the flowering of a rich disequilibrium non-methane hydrocarbon (NMHC) photochemistry in the cooler ($\sim$ 800 K) and presumptively metal-rich warm Neptune GJ 436b, but stopped short of concluding that the chemistry would necessarily lead to smogs. Moses and coworkers (Moses et al. 2011; Visscher and Moses 2011; Moses et al. 2013a,b; Moses 2014) extended this model to bigger molecules, concluding that "complex hydrocarbons and nitriles might produce high-altitude photochemical hazes" (Moses 2014). On the other hand, as Moses (2014) also points out, methane has not yet been seen in GJ 436b.

There are several other models of exoplanet thermochemistry and photochemistry that have been used to address a variety of hydrogen-rich exoplanets, from Jupiters to Neptunes to super-Earths, but none of them go as far as predicting the photochemical production of organic hazes. Venot et al. (2012) examined C-N-O photochemistry on HD 189733b and HD 209458b; Kopparapu et al. (2012) explored the effect of the C/O ratio on the hot Jupiter WASP-12b; Venot et al. (2013) used high-temperature UV cross sections to study the effect of CO_2 photolysis on the warm Neptune GJ 436b; Hu and Seager (2014) addressed temperature and elemental abundances in super-Earths and mini-Neptunes, with application to GJ 1214b, HD 97658b, and 55 Cnc e; Agúndez et al. (2014b) added tidal heating and metallicity variations to GJ 436b; Venot et al. (2014) looked at temperature, metallicity, UV flux, tidal heating, and atmospheric mixing in warm Neptunes, with application to GJ 3470b and GJ 436b; Miguel and Kaltenegger (2014) took into account stellar type and orbital distance; Miguel et al. (2015) focused on Lyman α irradiation of GJ 436b and other warm Neptunes; Koskinen et al. (2013) and Lavvas et al. (2014) addressed ion chemistry; Agúndez et al. (2012, 2014a) used a 2D model to address the horizontal quenching that occurs when winds carry hot air to cold places; and Benneke (2015) combined photochemistry with retrievals from exoplanet transit spectra to mine for C/O ratios in several planets.

Two recent models do include heavier organic molecules (Rimmer and Helling 2016; Venot et al. 2015). Rimmer and Helling (2016) compile an extensive reaction network that includes both

neutral and ion chemistry; they pay particular attention to the formation of prebiotic molecules like glycine, but they do not yet address photochemical hazes. Venot et al. (2015) have expanded their reaction network to include selected hydrocarbons with as many as eight carbon atoms. A plus is that their reaction network has been tested against combustion experiments. On the other hand, it should be borne in mind that complex models of complex systems often achieve empirical agreement by cancellation of errors, and that things can go awry when the model is applied to new conditions. Venot et al. (2015) compute that cyclohexadiene (cC_6H_8, an obscure but reasonably stable molecule) is a major photochemical product in 500 K stratospheres, exceeding even acetylene (C_2H_2) and CO in abundance. Although Venot et al. (2015) do not mention photochemical hazes, it is obvious that cyclohexadiene is well along the path to building a heavy smog. However, the stated pathway for cC_6H_8 formation goes through

$$C_2H_2 + C_2H_2 \rightarrow nC_4H_3 + H, \tag{R60r}$$

a very endothermic reaction that we will encounter again in section 4.1.1 when we discuss its reverse. We estimate that the rate for R60r is $k_{60r} = 3 \times 10^{-13} e^{-33000/T}$ cm^3/s, which at 500 K is very close to never. It is hard to imagine how a reaction with such a huge activation energy could actually be a major factor in a planetary atmosphere.

We have used our own code to address photochemistry and thermochemistry in giant planets and brown dwarfs Zahnle et al. (1995, 2009); Zahnle and Marley (2014). Early versions of this code (2011 and earlier) had some issues with the implementation of thermochemical equilibrium that were corrected after consultations with Channon Visscher. Miller-Ricci Kempton et al. (2012) and Morley et al. (2013, 2015) used the corrected code to address photochemistry in the warm ($T_{\rm eff} \approx 550$ K) super earth GJ 1214b and similar planets. They suggested that hazes should form when reduced organic radicals like CH_3 (building blocks of bigger organic molecules) were more abundant than OH. If so, NMHCs can be abundant enough that organic hazes show potential to provide a viable alternative to clouds of other condensible substances such as Na_2S. However, as with GJ 436b, methane has not been seen in GJ 1214b.

3. Model Details

We use a vanilla 1D kinetics code to simulate atmospheric photochemistry. Such codes parameterize vertical transport as a diffusive process with an "eddy diffusion coefficient," denoted K_{zz} [cm^2/s]. Volume mixing ratios f_i of species i are obtained by solving continuity

$$N\frac{\partial f_i}{\partial t} = P_i - L_i N f_i - \frac{\partial \phi_i}{\partial z} \tag{1}$$

and diffusion

$$\phi_i = b_{ia} f_i \left(\frac{m_a g}{kT} - \frac{m_i g}{kT} \right) - (b_{ia} + K_{zz} N) \frac{\partial f_i}{\partial z} \tag{2}$$

equations for each species. In these equations N is the total number density (cm^{-3}); $P_i - L_i N f_i$ represent chemical production and loss terms, respectively; ϕ_i is the upward flux; b_{ia}, the binary

115 diffusion coefficient between i and the background atmosphere a, describes true molecular diffusion;
116 and m_a and m_i are the molecular masses of a and i.

117 For the base model we use 481 forward chemical reactions and 42 photolysis reactions for 78
118 chemical species made from H, C, O, N, and S. We supplement these with 12 additional reactions
119 and two additional species for sensitivity tests. Every forward chemical reaction (e.g., $CO + OH \rightarrow$
120 $CO_2 + H$) is balanced by the corresponding reverse reaction (e.g., $CO_2 + H \rightarrow CO + OH$) at a
121 rate determined by thermodynamic equilibrium. We have not included reverses of the photolysis
122 reactions; that is, we include reactions such as $H_2O + h\nu \rightarrow H + OH$, but we do not include
123 $H + OH \rightarrow H_2O + h\nu$ because radiative recombination of small molecules is typically slow, and our
124 chemical system does not include large molecules for which radiative attachment can be important
125 (Vuitton et al. 2012).

126 Organic photochemistry begins with photolysis of methane. Methane fragments can react with
127 each other to make more complicated organic molecules. Non-methane hydrocarbons (NMHCs)
128 with unsaturated bonds are in turn prone to polymerizing to form chains, rings, PAHs (polycyclic
129 aromatic hydrocarbons), and soots (disorganized agglomerations of PAHs and sheets of PAHs). In
130 this study we truncate NMHC chemistry at C_2H_n, with the exception of C_4H_2. How we handle
131 C_4H_2 as a proxy for polymerization is discussed in detail in section 4.1.1 below. The more abundant
132 NMHC species in this model are C_2H_2, C_2H_4, C_2H_6, C_4H_2, H_2CO, CH_3OH, and HCN. The total
133 NMHC abundance is assessed as the total number of carbon atoms in the NMHCs and reported in
134 several figures below.

135 Sulfur photochemistry is the important new thing here. Sulfur photochemistry begins with
136 photolysis of, or chemical attack on, H_2S. Sulfur can be successively oxidized by OH (from H_2O
137 photolysis) to SO, SO_2, and SO_3 or H_2SO_4. Sulfuric acid (H_2SO_4) is a major aerosol on Venus and
138 Earth worth looking for generally. Sulfur can also react with hydrocarbons to make CS, CS_2, and
139 OCS. All three were abundant in the wake of the impacts of Comet Shoemaker-Levy 9 into Jupiter
140 in 1994 (Harrington et al. 2004). Finally, sulfur can polymerize, condense, and precipitate as the
141 element. The S_2 molecule was seen as a strong signature in the SL9 plumes (Moses et al. 1995;
142 Zahnle et al. 1995) and it has been seen in volcanic plumes over Io (Spencer et al. 2000). There is
143 strong circumstantial evidence in sulfur's isotopic record in Archean sediments that precipitation
144 of elemental sulfur was commonplace in the anoxic atmosphere of early Earth (Pavlov and Kasting
145 2002). Here we use a simplified system consisting of S, S_2, S_3, S_4, and S_8. As there is considerable
146 uncertainty in sulfur's reactions, we have listed our choices for key reactions in Table 1. Most of
147 the key reaction rates will be varied — and in one case, created — in sensitivity studies in section
148 5 below. All small sulfur-bearing molecules are rather easily photolysed but the sulfur rings —
149 here gathered together under the master ring S_8 — are more stable to UV (Young et al. 1983;
150 Kasting et al. 1989; Yung et al. 2009). Thus, as we shall see, there is a strong tendency for sulfur
151 to polymerize to S_8 under UV radiation.

152 The background atmosphere is assumed to be 84% H_2 and 16% He. The relative abundances of

C, N, O, and S are presumed solar and to scale as a group according to metallicity; scavenging of O and S by silicates and chalcophiles is taken into account (Lodders and Fegley 2006). For simplicity we assume solar metallicity in the base models (the star 51 Eridani itself is very slightly subsolar, [Fe/H] $= -0.027$). We consider one set of models with metallicity that is a Jupiter-like $3\times$ solar. It is not immediately obvious that higher metallicity always favors haze formation, despite the greater abundance of haze-forming elements. Indeed, in atmospheres where CH_4 is less abundant than CO, raising metallicity reduces the CH_4/CO ratio, and hence can make organic haze formation less favorable. Here we will find that raising the metallicity from solar to $3\times$ solar in 51 Eri b has a negative effect on NMHC formation.

51 Eridani is a bright star that was observed decades ago by the *International Ultraviolet Explorer* (*IUE*). We use the observed UV spectrum for $115 < \lambda < 198$ nm, the range of wavelengths for which data are available. For $\lambda > 198$ nm we use a standard stellar model photosphere for an F0IV star of radius $1.6R_\odot$, which makes the star's luminosity appropriate to 51 Eridani itself. We note in passing that the UV irradiation of 51 Eri b is about twice what it is at Earth today, or about $200\times$ what it is at Titan.

An important simplification is that we treat vertical mixing by an eddy diffusion parameter K_{zz} that does not vary with height. What K_{zz} should be in a stratified atmosphere like that of 51 Eri b is not well-constrained (Freytag et al. 2010). Values ranging from 10^3 cm^2/s at the top of the troposphere to $10^6 - 10^7$ cm^2/s at the top of the stratosphere seem to be useful for Jupiter (Moses et al. 2005), and values as high as 10^{10} cm^2/s have been suggested for hot Jupiters. Here we consider $10^5 \leq K_{zz} \leq 10^{10}$ cm^2/s.

We set surface gravity to $g = 32$ m/s^2 in the nominal model. To test the response of the model to different gravities we consider $g = 56$ m/s^2 as a variant. These bracket what is expected for 51 Eri b; $g = 32$ m/s^2 is not better than $g = 56$ m/s^2. The higher gravity models are cooler at a given pressure and thus are more favorable to CH_4 and to sulfur condensation.

The pressure-temperature profile is computed by a radiative-convective equilibrium model assuming a cloud-free atmosphere. In the troposphere these assumptions produce a relatively cool model. Unlike the thermal structure of the troposphere, which is governed by the planet's own luminosity, temperatures at very high altitude depend also on heating by the star. Here we simply extend an isothermal atmosphere to altitudes above the top of the radiative-convective model. This is an important limitation on our models: we don't know the temperature well enough to categorically state that sulfur does or does not condense in 51 Eri b. The temperature structure of a sulfurous atmosphere is a big enough topic that it is best deferred to a future study.

4. Results

We begin with a particular model that illustrates the general features of 51 Eri b photochemistry. We then look at how the models respond to parameter variations.
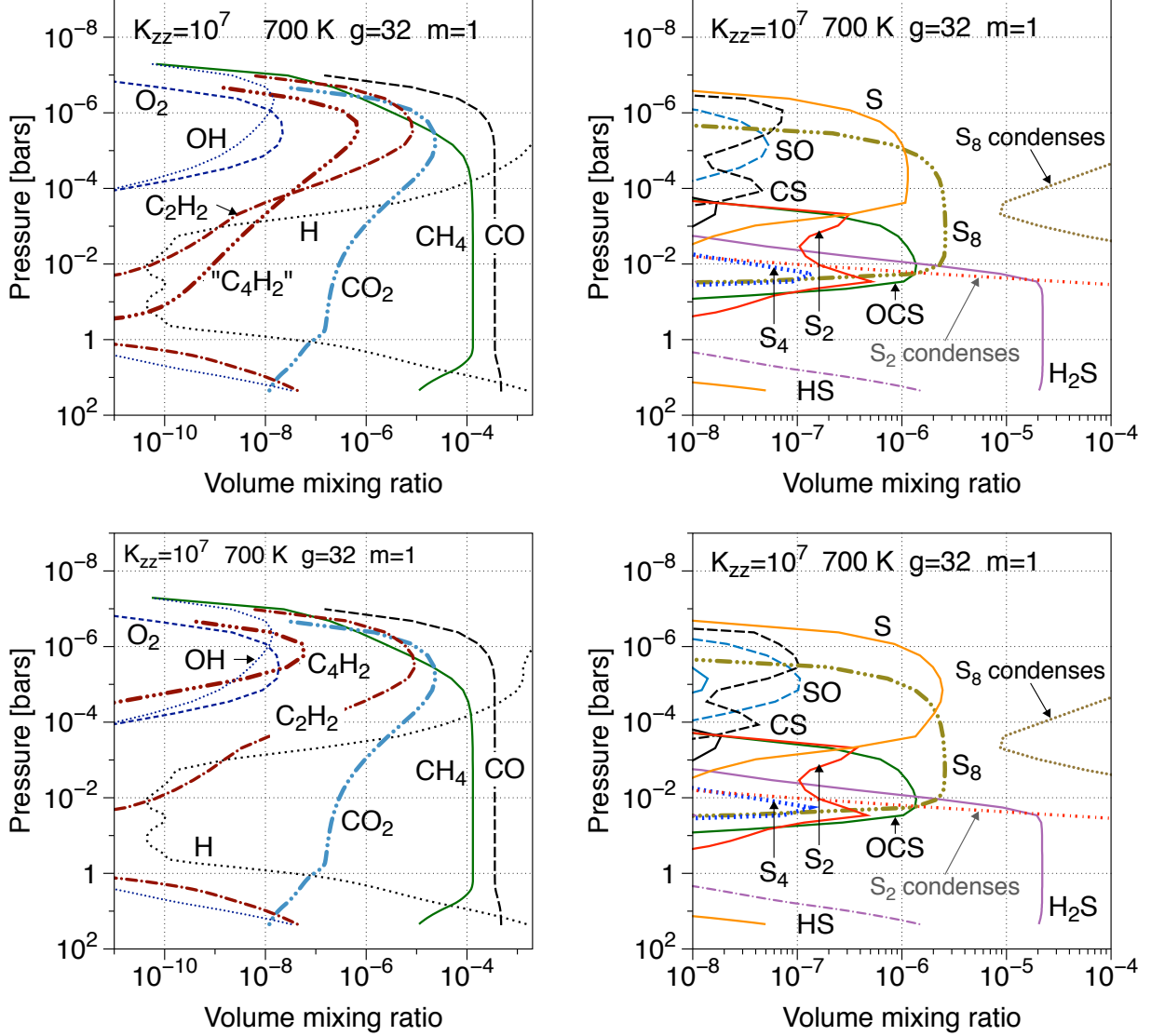
4.1. Nominal 51 Eri b models: two kinds

189

Fig. 1.— Photochemistry in a nominal 51 Eri b model (T_{eff} = 700 K, g = 32 m s^{-2}, solar metallicity, cloud-free atmosphere, K_{zz} = 10^7 cm^{2}s^{-1}). The top and bottom rows differ in how C$_4$H$_2$ is treated. How C$_4$H$_2$ is treated has little effect on the more abundant molecules. *Left.* Carbon and oxygen. In the top panel, "C$_4$H$_2$" is treated as the gateway to C$_2$H$_2$ polymerization. Where "C$_4$H$_2$" is more abundant than acetylene (C$_2$H$_2$), our chemical scheme has broken down. In the bottom panel, C$_4$H$_2$ is chemically recycled. *Right.* Sulfur shows a rich photochemistry that tends to build toward the relatively photolytically stable S$_8$ molecule. This particular model is about 5 K too warm for S$_8$ to condense. Abundances of SO, CS, and S in the upper stratosphere will be smaller than shown here if sulfur condenses. Note that S$_4$ is abundant at the interface between H$_2$S and S$_8$.

190   The particular model documented in Figure 1, which we call the nominal model, assumes an

191 effective temperature $T_{\text{eff}} = 700$ K, an eddy diffusivity of $K_{zz} = 10^7$ cm^{2}s^{-1}, constant gravity
192 $g = 32$ m/s^2, solar metallicity $m = 1$, and a cloud-free atmosphere. Figure 1 plots volume mixing
193 ratios of selected carbon-, oxygen-, and sulfur- bearing species as a function of altitude (pressure).
194 For carbon and oxygen we plot CO and CH$_4$, the major oxidized photochemical product CO$_2$, the
195 reduced photochemical products acetylene (C$_2$H$_2$) and C$_4$H$_2$, the bleaching agents OH and O$_2$, and
196 atomic H. For sulfur we plot most of the species that are abundant, although CS$_2$ and SO$_2$ are not
197 labeled and S$_3$, which is coincident with S$_4$ but less abundant in these models, is omitted entirely
198 for clarity. We do not plot H$_2$O (the most abundant molecule other than H$_2$), atomic O, other
199 hydrocarbons, nor any N-bearing species.

200 Figure 1 illustrates the vertical structure of chemical products. The top of the atmosphere is
201 relatively oxidized by OH from H$_2$O photolysis, but it is also where CH$_4$ is photolyzed by Lyman
202 α, and so the top is also the primary source of small hydrocarbon radicals. Reactions with OH
203 are the chief competition to hydrocarbon polymerization because the CO bond once formed is
204 effectively unbreakable in the haze-forming region. Thus NMHC production is possible only when
205 OH is suppressed. OH is controlled by reaction with H$_2$ to reconstitute H$_2$O, or with CO to make
206 CO$_2$; this is why CO$_2$ is always a major photochemical product in all 51 Eri b models. Conditions
207 are more reduced at greater depth.

4.1.1. Alternative carbon polymerizations

209 It is self-evident that hydrocarbon polymerization can ramify without any known limit, espe-
210 cially in the presence of nitrogen and a little oxygen. In the bigger picture this is obviously a good
211 thing, but our modeling effort cannot ramify without limit. We must either be able to show that
212 abundances go to zero for molecules with more than a few carbon atoms, or we must artificially
213 truncate the system. If the atmosphere is sufficiently oxidized, the first option is workable. The
214 system will stop at CO$_2$ without much of interest happening — this has historically been the bane
215 of terrestrial prebiotic atmospheric chemistry models (Abelson 1966; Pinto et al. 1980). But here
216 we are dealing with H$_2$-rich atmospheres and it is not obvious *a priori* that the chemistry converges.

217 In this study we truncate the system at C$_4$H$_2$, the first molecule to form as the product of two
218 C$_2$H$_n$ molecules. The state of the art in exoplanets takes the chemistry up to C$_8$H$_n$ (Moses 2014;
219 Venot et al. 2015; Rimmer and Helling 2016), but only a tiny fraction of all possible C$_m$H$_n$ (m $\leq$ 8)
220 can be taken into account, and the combinatorial nature of the chemistry rapidly approaches or
221 exceeds the limit of what can be done with a detailed chemical kinetics model. Further progress
222 requires working with a limited number of generic or representative species. We consider two
223 extreme assumptions that might bound the problem.

224 In one set of numerical experiments we treat C$_4$H$_2$ as a bucket in which polymerizing carbon
225 accumulates, rather than as an actual chemical species. The only loss is the reverse of the formation

226 reaction,

$$C_2H + C_2H_2 \rightarrow C_4H_2 + H. \tag{R57}$$

227 The underlying idea is that C_4H_2 is destined to grow into ever larger $C_mH_nN_xO_yS_z$ molecules by
228 the addition of free radicals. When used in this way, we will from here forward put quotes on
229 "C_4H_2" to indicate that we are treating it as a representative species rather than as the real C_4H_2
230 molecule. This is the case documented by the upper left-hand panel of Figure 1 and in most other
231 spaghetti plots in this paper.

232   In the other set of numerical experiments we add three chemical reactions with H to crack
233 C_4H_2: first an addition,

$$C_4H_2 + H + M \rightarrow C_4H_3 + M \tag{R58}$$

234 followed either by H-abstraction

$$C_4H_3 + H \rightarrow C_4H_2 + H_2 \tag{R59}$$

235 or by fission

$$C_4H_3 + H \rightarrow C_2H_2 + C_2H_2. \tag{R60}$$

236 Reaction R58 is a fast reaction that has been studied both theoretically and experimentally (Eite-
237 neer and Frenklach 2003; Klippenstein and Miller 2005); we use rates for k_{58} from the latter. The
238 other two reactions are inventions. For R59, we assume that $k_{59} = 5 \times 10^{-11} \exp\left(-500/T\right)$ cm^3/s,
239 which is not unusual for an H-abstraction, if perhaps a bit fast. For R60, the unusual reverse
240 reaction R60r discussed above with respect to cyclohexadiene suggests that there ought to be a
241 considerable activation barrier and a rather small collision factor to the reverse reaction to account
242 for the special geometry that would seem required. We assume that

$$k_{60} = 5 \times 10^{-11} \exp\left(-2000/T\right) \quad \text{cm}^3/\text{s}. \tag{3}$$

243 The lower left-hand panel of Figure 1 shows that adding reactions R58-R60 to the network reduces
244 the peak abundance of C_4H_2 and restricts the molecule to the photochemical region. Not shown is
245 that if k_{60} is reduced by a factor of 30, the C_4H_2 altitude profile reverts to the "C_4H_2" profile seen
246 in the upper left panel of Figure 1.

247   We note that neither R59 nor R60 are likely to be important in reality. Much more likely is
248 that the reaction with H will be another addition (Harding et al. 2007) and the hydrocarbon will
249 continue to grow,

$$C_4H_3 + H + M \rightarrow C_4H_4 + M, \tag{R61}$$

250 with no natural truncation point in the photochemical region where C-bearing radicals are also
251 abundant; that is, additions and ramifications will continue, and there is no obvious end to this.
252 From this perspective "C_4H_2" is a gateway species. At greater depth in a hydrogen-rich atmosphere,
253 hydrogenation will probably focus on the unsaturated carbon bonds until what is left is an alkane
254 or alkanes, and in the end the alkanes will be hydrogenated to CH_4 and H_2, completing the cycle.

255   In most figures that follow we will show "C_4H_2" profiles computed with the high C_4H_2 because
256 these are more interesting to look at.

4.1.2. Sulfur photochemistry and sulfur condensation

The righthand panels of Figure 1 line up the sulfur chemistry with the carbon and oxygen chemistry in the nominal model. Several things stand out. The first is that H_2S — sulfur's stable form in the abyss — barely makes it past the tropopause. Although H_2S is susceptible to UV photolysis, that is not what is happening here. Rather, H_2S is being destroyed by atomic H flowing down from the high altitude photochemical source region,

$$H_2S + H \rightarrow HS + H_2. \tag{R23}$$

The HS radical reacts quickly with H to free S,

$$HS + H \rightarrow S + H_2, \tag{R9}$$

and atomic S reacts with HS to make S_2,

$$HS + S \rightarrow S_2 + H, \tag{R8}$$
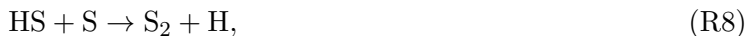
and the polymerization of sulfur has begun, which is the second thing to stand out: S_8 is very abundant, generally at a lower altitude than the NMHCs and under more reduced conditions.

The high predicted abundance of S_8 suggests that it might condense. Sulfur vapor is complicated by the presence of several allotropes. Our first simplification is to lump S_6 and S_7 together with the more abundant S_8. Lyons (2008) gives simple curve fits to many allotropes above the liquid, and then describes a scheme for extrapolating these to lower temperatures above solid sulfur. A complication is that the vapor pressure curves given by Lyons (2008) are discontinuous by nearly a factor of two at sulfur's melting point ($T_m = 398$ K). We use a blended approximation in which the vapor pressure over the solid is extended to higher temperature until it intersects the reported vapor pressure over the liquid,

$$p_v(S_8) = \exp\left(20 - 11800/T\right) \qquad T < 413 \text{ K}$$

$$p_v(S_8) = \exp\left(9.6 - 7510/T\right) \qquad T > 413 \text{ K} \tag{4}$$

where the vapor pressure is in bars. In Figure 1, the S_8 mixing ratio is $\sim 2 \times 10^{-6}$ for atmospheric pressure levels between 100 μbars and 10 mbars. At these partial pressures, $2 \times 10^{-10} < p(S_8) < 2 \times 10^{-8}$, sulfur's condensation temperature is between 280 and 310 K. The uncertainty in Eq 4 in this temperature range is probably less than a factor of two (the coldest datum is at ~ 310 K), which is insignificant compared to the uncertainty in the temperature in our models. For context, the corresponding condensation temperatures for water are between 170 and 200 K at the same altitudes. At higher metallicity both condensation temperatures are $\sim 20 \log_{10}(m)$ K higher.

The vapor pressure of S_2 over solid or liquid sulfur is tiny (Lyons 2008),

$$p_v(S_2) = \exp\left(27 - 18500/T\right) \qquad T < 413 \text{ K}$$

$$p_v(S_2) = \exp\left(16.1 - 14000/T\right) \qquad T > 413 \text{ K.} \tag{5}$$

All of our models of 51 Eri b predict more S_2 than would be consistent with the presence of condensed sulfur. Evidently S_2 (and S_3 and S_4 as well) would be drawn down to negligible amounts where S_8 condenses.

Saturation mixing ratios of S_8 and S_2 over solid sulfur are plotted on Figure 1. A third thing stands out: S_8 in 51 Eri b is very close to its condensation point. In this particular model S_8 does not condense, but if the model were a few degrees cooler it would condense. If S_8 condenses, we can presume that there would be much less S_2, SO, CS, and S above the clouds than is shown here.

4.2. Dependence on vertical mixing

In this study vertical mixing is a free parameter. Figure 2 shows what happens when K_{zz} is made much bigger or much smaller. These are high "C_4H_2" models. Strong vertical mixing ($K_{zz} = 10^9$ cm^{2}s^{-1}, top panels) creates a more oxidized environment at the top of the atmosphere that is unfavorable to NMHC growth. In particular, "C_4H_2" is all but wiped out. Weak vertical mixing ($K_{zz} = 10^5$ cm^{2}s^{-1}, bottom panels) is more favorable to NMHCs, especially at lower altitudes that are too deep for oxidants to reach when the mixing is weak. This is somewhat obscured by our plotting volume mixing ratios in Figure 2, which exaggerates the apparent importance of trace species at high altitudes, and understates the importance of anomalies at $K_{zz} = 10^5$ cm^{2}s^{-1}. In fact $K_{zz} = 10^5$ cm^{2}s^{-1} is more conducive to hydrocarbon polymerization than is $K_{zz} = 10^7$ cm^{2}s^{-1}.

The effects of changing K_{zz} on sulfur are parallel to those on carbon but more exaggerated. Strong vertical mixing (Figure 2, upper right-hand panel) enables H_2S to get higher before it gets destroyed, which creates a more favorable environment for S_2, which becomes rather abundant. If S_8 does not condense, eddy mixing also lifts it to high altitudes where it is photolyzed and oxidized to SO and SO_2 or reduced to CS. Weak vertical mixing (Figure 2, lower right-hand panel) squeezes the sulfur photoproducts into a relatively thin region below the homopause and above the H_2S destruction horizon at 30 mbars; the high molecular weight of S_8 prevents sulfur getting very high, which markedly depletes the top of the atmosphere in all sulfur species even if sulfur does not condense.

4.3. Dependence on effective temperature

Figure 3 shows what happens when the effective temperature of the planet is raised or lowered by 50 K. These are high "C_4H_2" models. The cooler atmosphere is clearly more oxidized. In carbon this is seen in the higher abundance of CO_2 and the lower abundances of C_2H_2 and "C_4H_2," in sulfur it is seen in higher abundance of SO and SO_2 and the disappearance of CS. The primary oxidant is OH from H_2O photolysis. The most important sink on OH is the temperature-sensitive
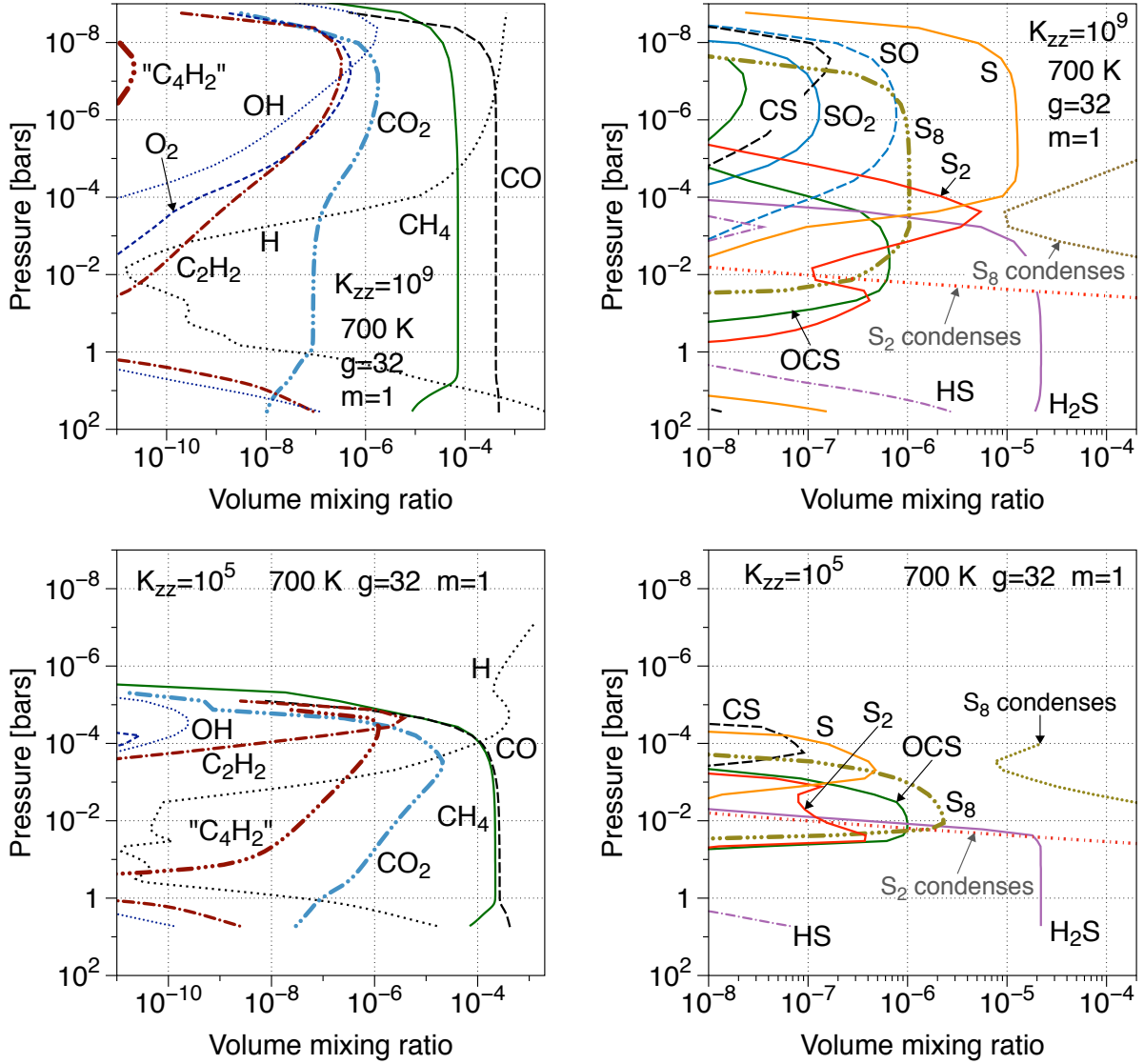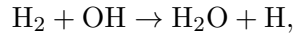
Fig. 2.— The effect of K_{zz} on carbon and sulfur photochemistry in our nominal 51 Eri b model. Mixing is $100\times$ stronger (top row) and $100\times$ weaker (bottom row) than in Figure 1 (these are both high "C_4H_2" models to be compared to the top panels of Figure 1). High vertical mixing creates a more oxidized environment at the top of the atmosphere that is less favorable to S_8 and very unfavorable to NMHC growth. Strong vertical mixing is more favorable to S_2, SO, and SO_2, less favorable to S_8. Weak vertical mixing produces a more reduced atmosphere that is more favorable to NMHCs and to S_8, which forms abundantly in deeper, warmer regions.

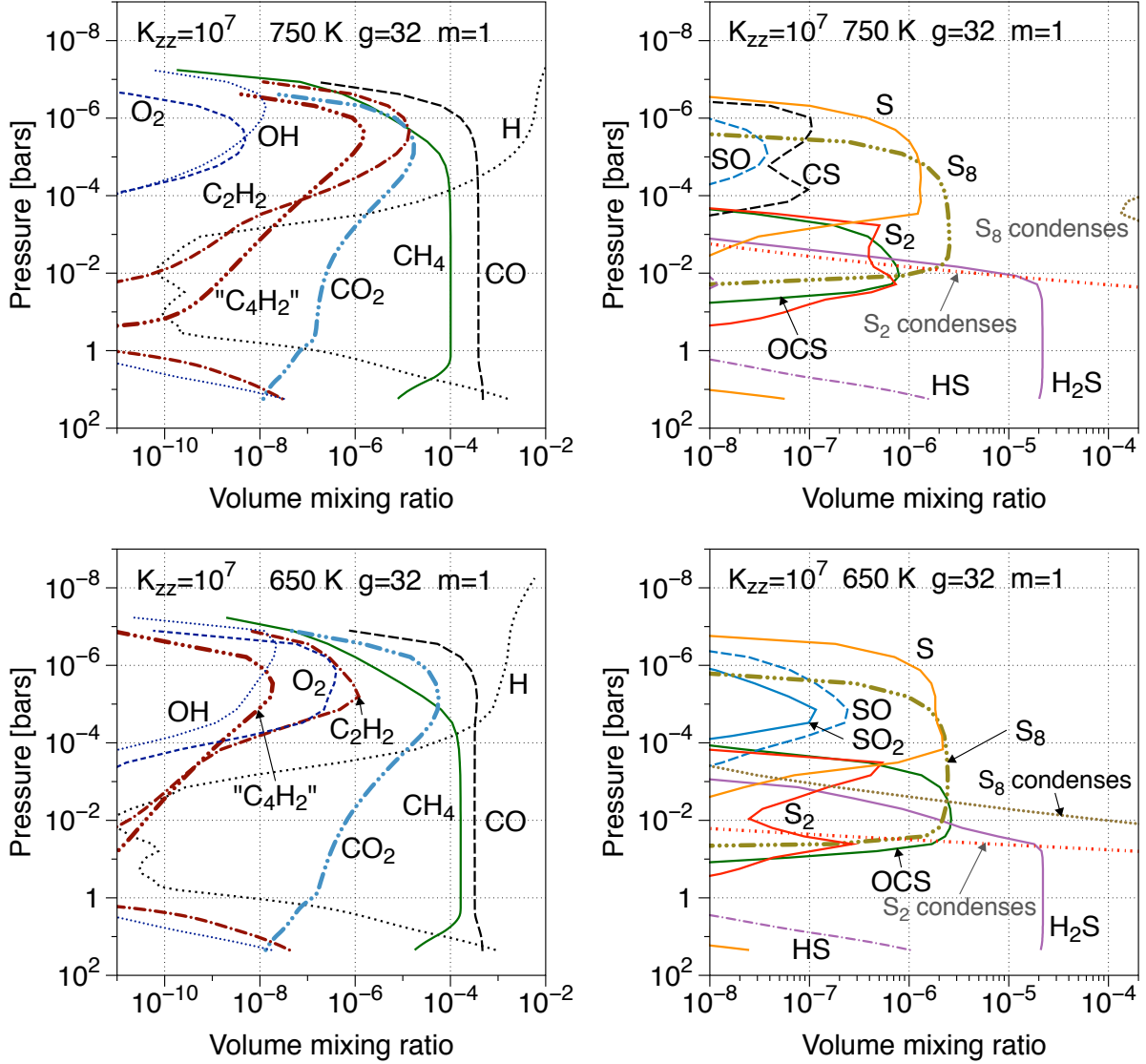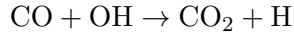317 reaction with H_2

$$H_2 + OH \rightarrow H_2O + H,$$

Fig. 3.— The effect of temperature on carbon and sulfur photochemistries. These are 50 K hotter (top) or colder (bottom) than the corresponding model high C_4H_2 model in Fig 1. Note that the $T_{\rm eff} = 650$ K (lower panels) models are more oxidized and less favorable to NMHCs. Note that S_8 condenses in the cooler models but does not condense in the warmer.

which puts H_2O back together. The high abundance of H_2 in a solar composition gas ensures that the reaction with H_2 is the leading sink on OH for $T > 200$. It is only where $T < 200$ K that the temperature-insensitive reaction with CO,

$$CO + OH \rightarrow CO_2 + H$$

becomes more important, but we do not encounter temperatures this low in 51 Eri b models. The reaction with H_2 becomes much slower as the temperature drops and consequently the OH

abundance becomes much larger as the temperature drops. In turn the higher OH abundance promotes CO_2 formation and inhibits NMHC growth. Both trends are clearly seen in the lower panels of Figure 3.

The other effect of temperature on sulfur is the obvious one that condensation becomes more likely in the cooler models. Sulfur readily condenses in the cooler $T_{eff} = 650$ K model at around 3 mbar (Figure 3, lower right-hand panel). This is also the altitude where organic hazes would form if any do, if the proxy "C_4H_2" is a useful guide.

4.4. Overview of carbon chemistry

Figure 4 gives an overview of carbon photochemistry for solar composition models over the phase space of different T_{eff}, g, and K_{zz} pertinent to 51 Eri b. We consider temperatures of $T_{eff} = 750$ K and $T_{eff} = 650$ K in addition to the nominal model with $T_{eff} = 700$ K, and we consider a gravity of $g = 56$ m/s^2 in addition to the nominal $g = 32$ m/s^2. Figure 4 is restricted to solar metallicity and the UV radiation observed by *IUE*. We vary K_{zz} between 10^5 cm^2/s and 10^{10} cm^2/s for all variants of T_{eff} and g.

Figure 4 plots the quenched disequilibrium CO and CH_4 mixing ratios and it plots the peak mixing ratios reached by the major photochemical products. 51 Eri b is near the boundary between CO-dominated and CH_4-dominated atmospheres (in equilibrium, the carbon would almost entirely be in CH_4). Both gases are abundant in all models, although CO is more abundant in most of them. In general, CH_4 is most abundant when K_{zz} is small, or the gas cooler, or the gravity higher (Zahnle and Marley 2014). None of the cases are truly methane-rich.

Smaller values of K_{zz} are more favorable to photochemical NMHC formation and high values of K_{zz} are very unfavorable. The apparently lower NMHC production at low values of K_{zz} is illusory, a consequence of plotting peak mixing ratios in Figure 4. The peak occurs at higher pressure at $K_{zz} = 10^5$ cm^{2}s^{-1} than at $K_{zz} = 10^7$ cm^{2}s^{-1}, so that NMHC densities at $K_{zz} = 10^5$ cm^{2}s^{-1} are actually higher. Some of the trend with K_{zz} can be ascribed to the CH_4/CO ratio, but the trend is even stronger in CO_2, which suggests that the weaker mixing is also acting to isolate and preserve the photochemical products. On the other hand, the relative dearth of NMHCs in the cooler $T_{eff} = 650$ K models is a real feature caused by the strong temperature dependence of the $H_2 + OH \rightarrow H_2O + H$ reaction that holds OH in check.

4.5. Overview of sulfur chemistry

Figure 5 presents the corresponding overview of sulfur photochemistry. Here we count sulfur atoms, so that S_2 is counted doubly and S_8 is counted eight-fold. The symbols are not like pie charts. They do not show how sulfur is apportioned at any one height. Rather, they show each
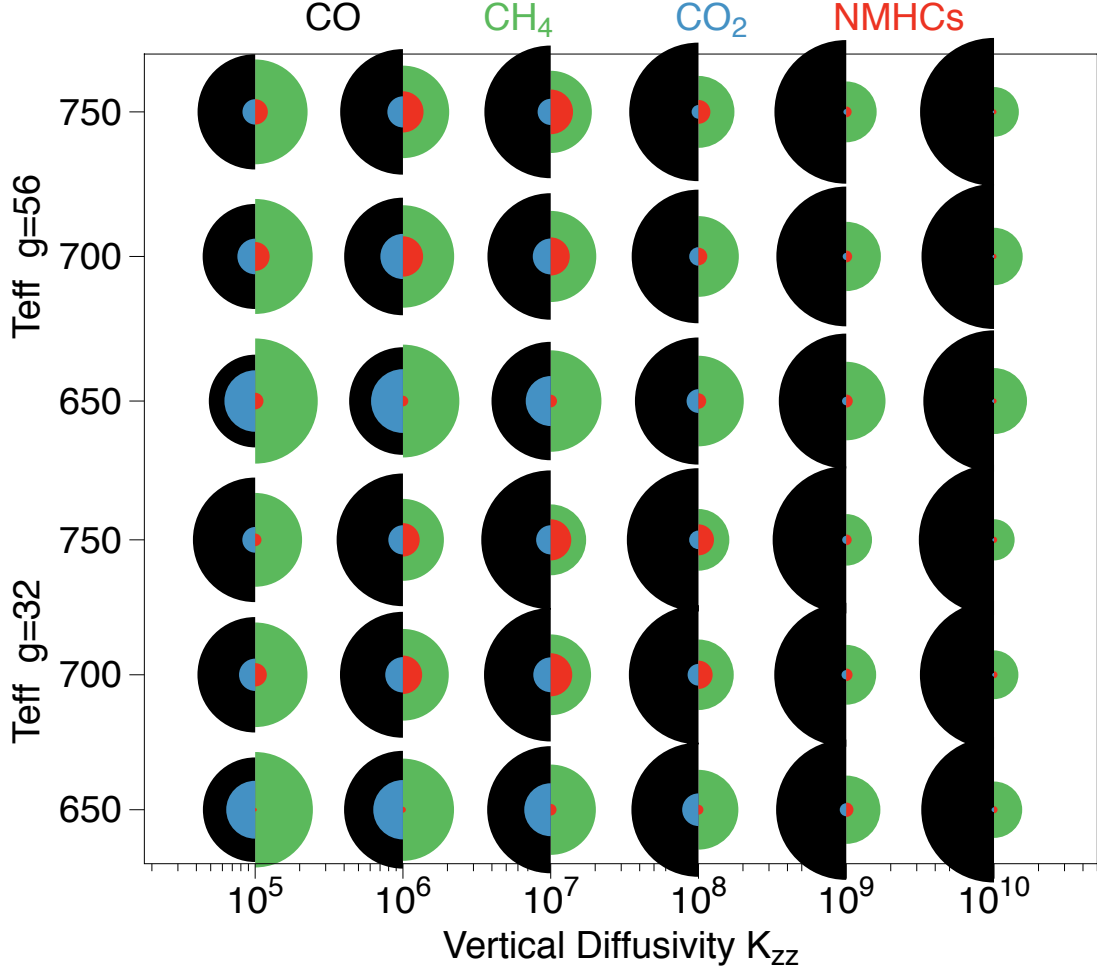
Fig. 4.— Carbon photochemistry in some possible 51 Eri b's of solar metallicity subject to the observed *IUE* UV flux from 51 Eri a. Peak volume mixing ratios are plotted in proportion to the areas of the disks. CO (black) and CH$_4$ (green) are quenched disequilibrium abundances welling up from below. The photochemical products CO$_2$ (blue) and NMHCs (red, chiefly C$_2$H$_2$) are maxima found at higher altitudes where photochemistry is king.

category at its peak abundance, which in most cases are at different heights. In this way we see that, for example at $K_{zz} = 10^7$, almost all the sulfur transitions from H$_2$S to S$_8$ at higher altitudes, or that at $K_{zz} = 10^{10}$, almost all the sulfur that started in H$_2$S is found in S$_2$ higher up and then still higher up it is found as S.

Several trends are evident in Figure 5. One is that H$_2$S is quantitatively converted to elemental sulfur. For weaker vertical mixing the sulfur will pool in S$_8$. The OCS molecule will be abundant. Strong vertical mixing favors S$_2$ and S. As with carbon, the cooler atmospheres are more strongly oxidized, but with sulfur the more strongly oxidized species are more prevalent when the vertical
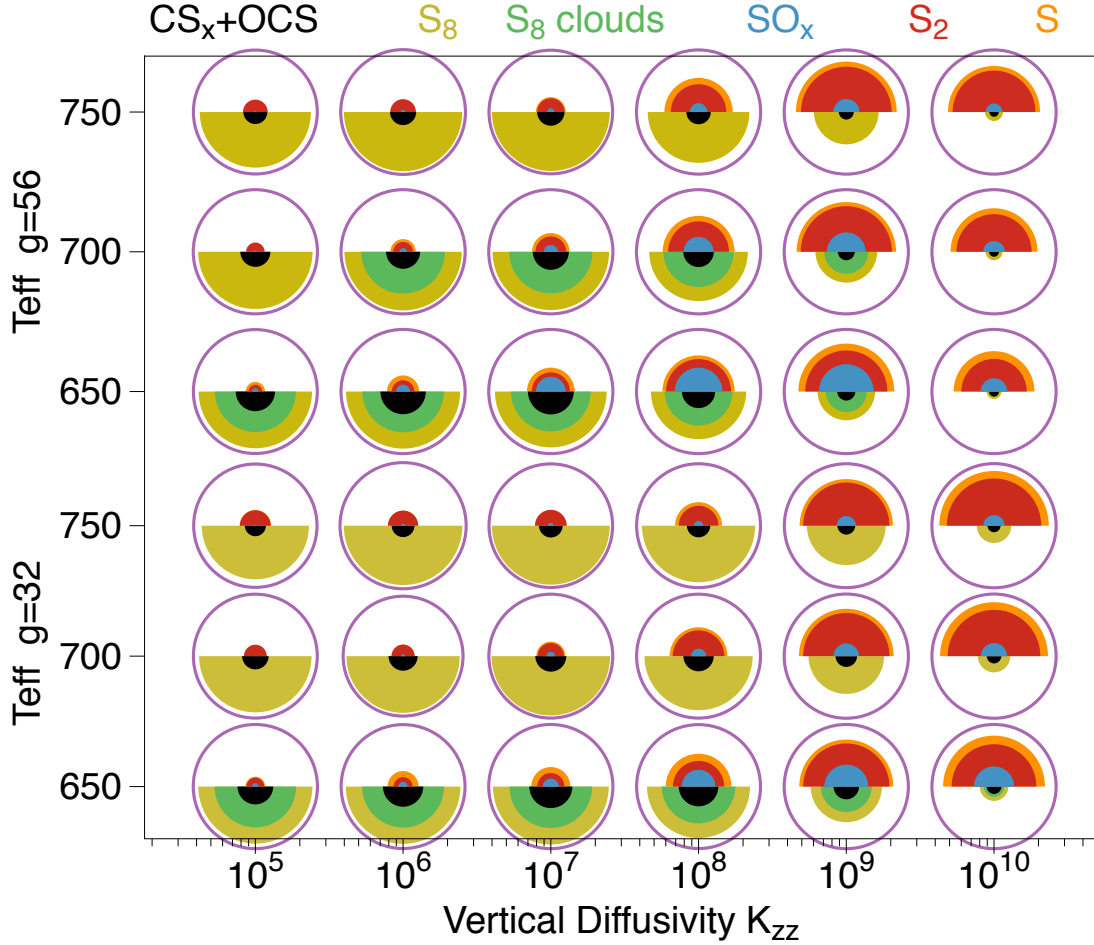
Fig. 5.— Overview of sulfur photochemical products. Sulfur is grouped into relatively oxidized species (SO and SO_2), carbonized species (mostly OCS), and two allotropes of elemental sulfur (S_2 and S_8). The circles and semicircles represent maximum mixing ratios as the areas of the implicit disks. The outer ring is the mixing ratio of H_2S in the deep atmosphere. In cooler models S_8 is predicted to condense; in these half of the S_8 is colored green.

mixing is stronger because when mixing is weak S_8 settles out, as was seen in the bottom-right panel of Figure 2. About half the models predict that sulfur condenses in clouds.

4.6. Metallicity

Figure 6 illustrates the effect of higher metallicity $m = 3$ in the $g = 32$ m/s^2 models as a function of K_{zz} for both carbon and sulfur chemistry. In this figure the carbon and sulfur mixing ratios are plotted to the same scale to facilitate cross-comparison, but as a consequence sulfur's circles are rather small. In order to see both S_2 and S, these are plotted as quarter circles. As

is well-known, higher metallicity strongly favors CO and CO_2 over CH_4. Higher metallicity has little effect on sulfur speciation because (i) all of its major products are metal-rich and (ii) its most abundant product, S_8, is the metal-richest.
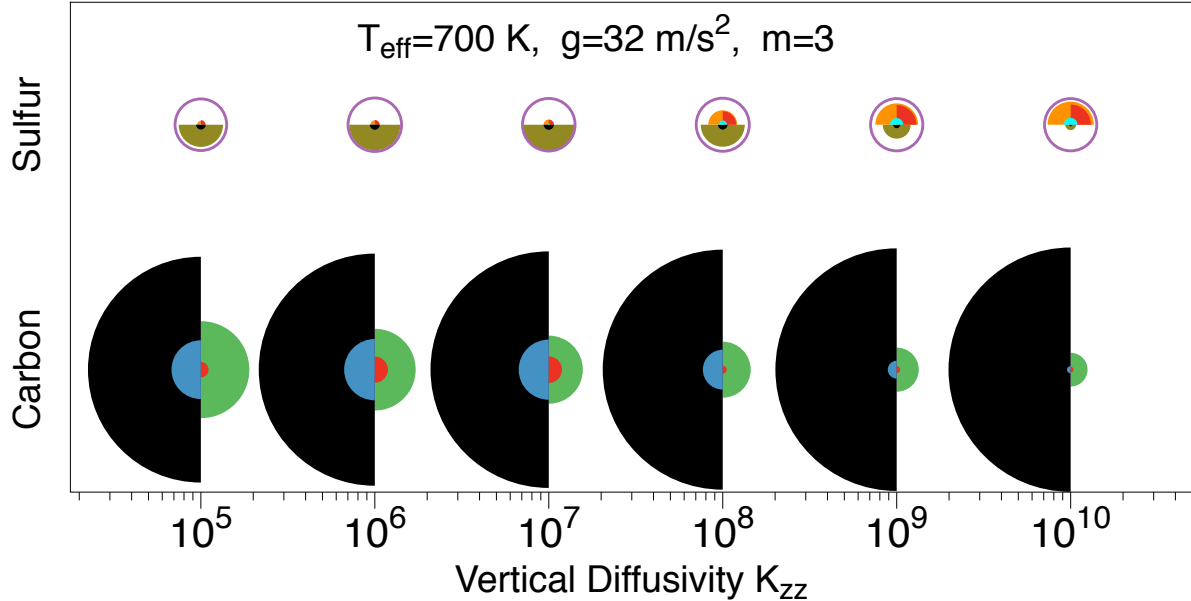

Fig. 6.— Higher metallicity ($m = 3$). Symbols and colors have the same meaning as in Figures 4 and 5 above. On this figure we plot sulfur and NMHC mixing ratios to the same scale to facilitate direct comparison.

4.7. Optical depths

It is possible that sulfur will be optically thick when it condenses, and it is possible that several of its optically-active allotropes will be visible when it does not. Here we estimate the optical depths of sulfur clouds and of sulfur vapor through the S_4 di-radical, and we give an optimistic estimate of the opacity from organic hazes.

For the sulfur clouds we gather all the S_8 above the condensation height into either 1 or 10 μm diameter particles, a size range that seems appropriate for condensation clouds. We assume effective particle densities of 1.5 g/cm^3. Both optical depths are shown in Figure 7 as gold and green disks, respectively. For S_4 we show the optical depth at 500 nm (red disks), which is near the center of its strong broadband visible light absorption.

For the organic hazes, we consider two cases. The first (black disks) is based on NMHC mixing ratios: we presume that 10% of the NMHCs (chiefly C_2H_2) go into haze particles at altitudes where the total mixing ratio of NMHC's exceeds 1 ppmv. The second case (gray disks) is based on the
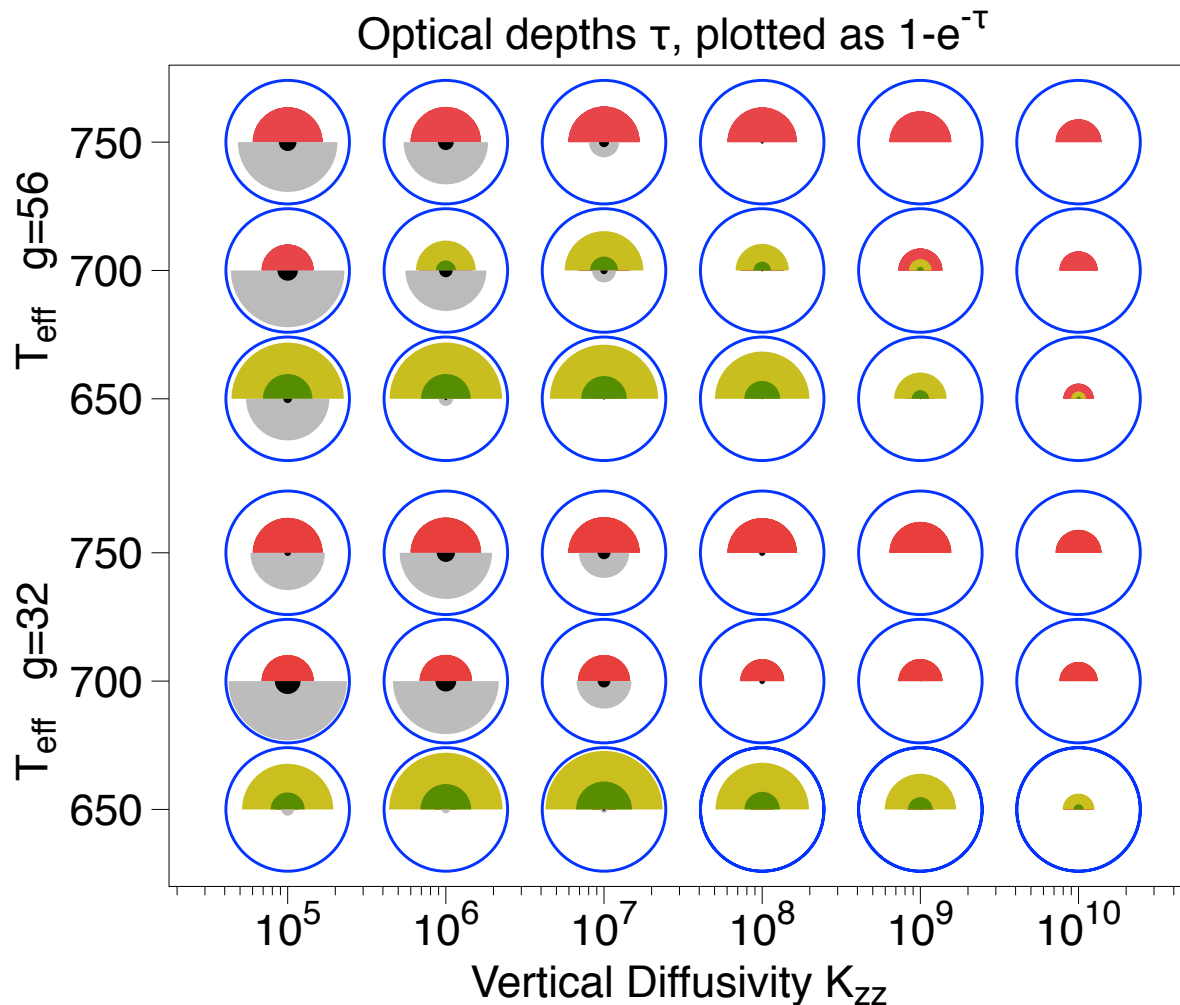
Fig. 7.— Optical depths at a glance. We plot $1 - e^{-\tau}$ rather than τ itself to give a better graphical sense of how much light is blocked. The outer circle represents the incident light. The black and gray disks show two upper bounds on clouds of 100 nm diameter organic particles. Black is deduced from mixing ratios in the photochemical zone where acetylene peaks, while gray refers to number densities of "C_4H_2," which typically peaks deeper in the atmosphere. Gold shows clouds of 1 micron diameter sulfur particles and green shows clouds of 10 micron diameter sulfur particles. Cherry red disks show the optical depth of S_4 vapor at 500 nm. Where sulfur condenses, S_4 should condense too, and so it is not shown. Results are for solar composition; τ for sulfur scales with metallicity but τ of organic hazes may not.

387 computed number densities of "C_4H_2" when treated as a portal through which every carbon that
388 passes ultimately gets incorporated in a haze particle. For both cases we assume that organic
389 particles are 100 nm diameter and of effective density 0.6 g/cm^3.

390   The results of the exercise are presented in Figure 7 for the same range of solar composition
391 models discussed above. Sulfur is in the top hemisphere of each circle and carbon in the bottom

half. There appears to be considerable potential for sulfur to be optically significant in 51 Eri b. This can be as sulfur clouds if 51 Eri b is a cool object, or as vapor if sulfur does not condense. The sulfur clouds can be optically thick at solar metallicity, and they could be significantly thicker on planets because sulfur optical depths will scale linearly with metallicity. The sulfur vapors can also be important, especially the chains. E.g., S_4 absorbs strongly at 500 nm, and longer chains absorb to 750-850 nm (Meyer 1976) (the rings, which confer invisibility, typically absorb $\lambda < 330$ nm). It is well known that liquid sulfur when heated turns from light yellow to dark red as S_8 rings decompose into a soup of chains and rings (the depth of red depends on impurities, especially hydrocarbons (Moses and Nash 1991)). We might expect similar behavior in 51 Eri b as S_8 rings thermochemically decompose between 10 and 100 mbars. On the other hand sulfanes, alkane analogs with the general formula HS_nH, may be the intermediaries between S_8 and H_2S; like the rings, sulfanes typically absorb $\lambda < 330$ nm (Meyer 1976).

There is also some potential for organic hazes to be important, especially where K_{zz} is small, but this potential is model dependent. At high altitudes where CH_4 and H_2O are photolyzed, optical depths near unity (black disks) are achievable only if conversion of acetylene into PAHs is highly efficient, which seems unlikely. Lower altitudes that coincide with the more reduced S_n-H_2S photochemistry are more promising, but interpreting "C_4H_2" as a bucket full of particles is a leap that future work could prove baseless. A difference from sulfur is that we do not expect that modestly higher metallicity will lead to more organic haze.

5. Sensitivity of the results to model uncertainties

We have found that most of our models predict that S_8 is a major product of sulfur photolysis (Figure 5). We have also found that NMHC formation is sensitive to sulfur photochemistry. We have discussed truncation of hydrocarbon chemistry at C_4H_2 above. Here we perform a series of tests to determine how sensitive the model is to other uncertain or unknown factors. These are (i) different amounts of stellar ultraviolet radiation; (ii) different rates of S_8 photolysis; (iii) different estimates of H_2S thermolysis and recombination; (iv) different rates of sulfur polymerization; and (v) unknown chemical reactions that would compromise S_8's stability. The latter proves the matter of most concern.

5.1. Sensitivity to UV

In Figure 8 we have explored the sensitivity of the nominal model to reduced levels of UV radiation. With UV irradiation at 10% that in the nominal model, the general pattern of the photochemistry is similar to that in the nominal model. Chief differences are that there is less CO_2 and C_2H_2, H_2S reaches higher altitudes before it is destroyed, and there is a modest shift away from S_8 as the chief product. Even when the UV is reduced to 0.1% that of the nominal model, there
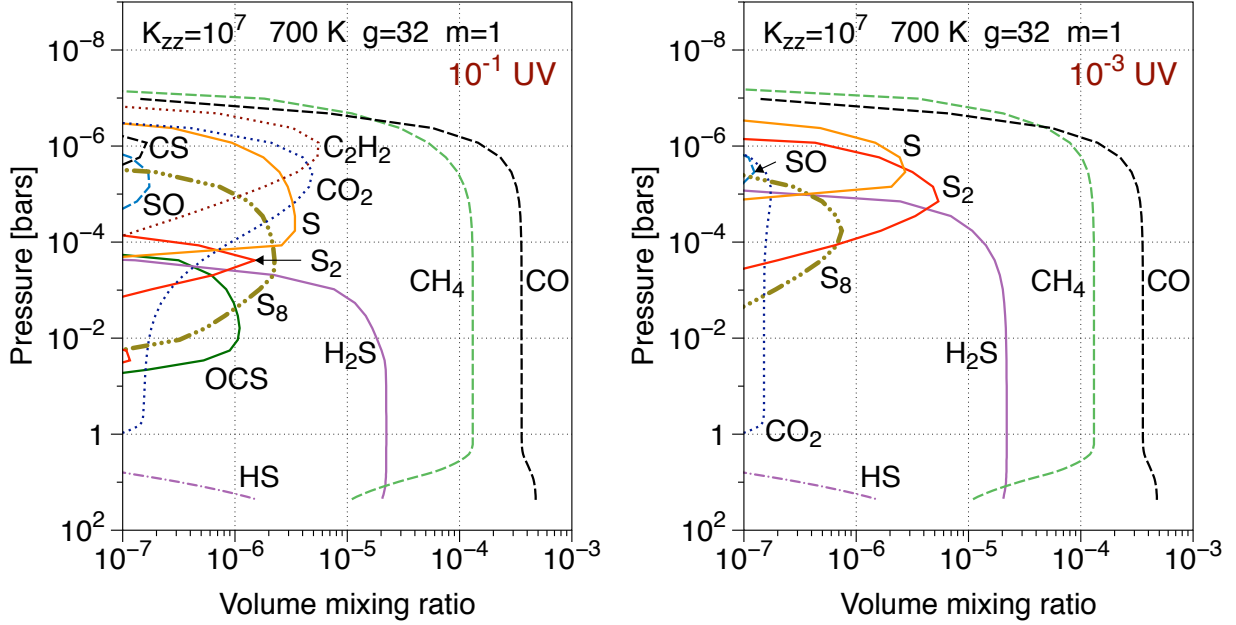
Fig. 8.— 51 Eridani b models with reduced and greatly reduced UV irradiation. *Left.* UV irradiation is 10% that in the nominal model. *Right.* UV irradiation is reduced to 0.1% that in the nominal model. Photochemical CO_2 and C_2H_2 nearly disappear, but a rich sulfur photochemistry remains.

are enough photons for H_2S to be fully consumed and a complete suite of sulfur photochemical products is generated. It is only when UV irradiation is reduced by another factor of ten that most of the H_2S survives and the sulfur photochemistry becomes photon-limited.

5.2. Sensitivity to S_8 photolysis

We have used Young et al. (1983)'s method for estimating S_8's photolysis rate. Young suggested that the first UV photon absorbed cleaves the ring. The resulting linear S_8 molecule can either be put back into the form of a ring by a collision, or it can be broken into two pieces (here both S_4) by absorbing a visible light photon. We assume an absorption cross section of 3×10^{-18} cm^2 to visible light ($\lambda < 850$ nm, Meyer 1976). The effective photolysis rate is

$$P(S_8) = P(S_{8,r}) \frac{N_c P(S_{8,l})}{N_c P(S_{8,l}) + \nu_c}, \tag{6}$$

where $P(S_{8,r})$ and $P(S_{8,l})$ are the photolysis rates of the ring and linear S_8 molecules, respectively; N_c is the number of collisions required to close the ring; $\sigma_c = 3 \times 10^{-15}$ cm^2 is the collision cross section of a molecule; and $\nu_c = N\sigma_c\bar{v}$ is the collision frequency in terms of the mean thermal speed $\bar{v}$. In the nominal model we take $N_c = 1$. For the sensitivity test (Figure 9) we take $N_c = 30$. The chief consequence of higher S_8 photolysis is that catalytic sulfur is more abundant and NMHC
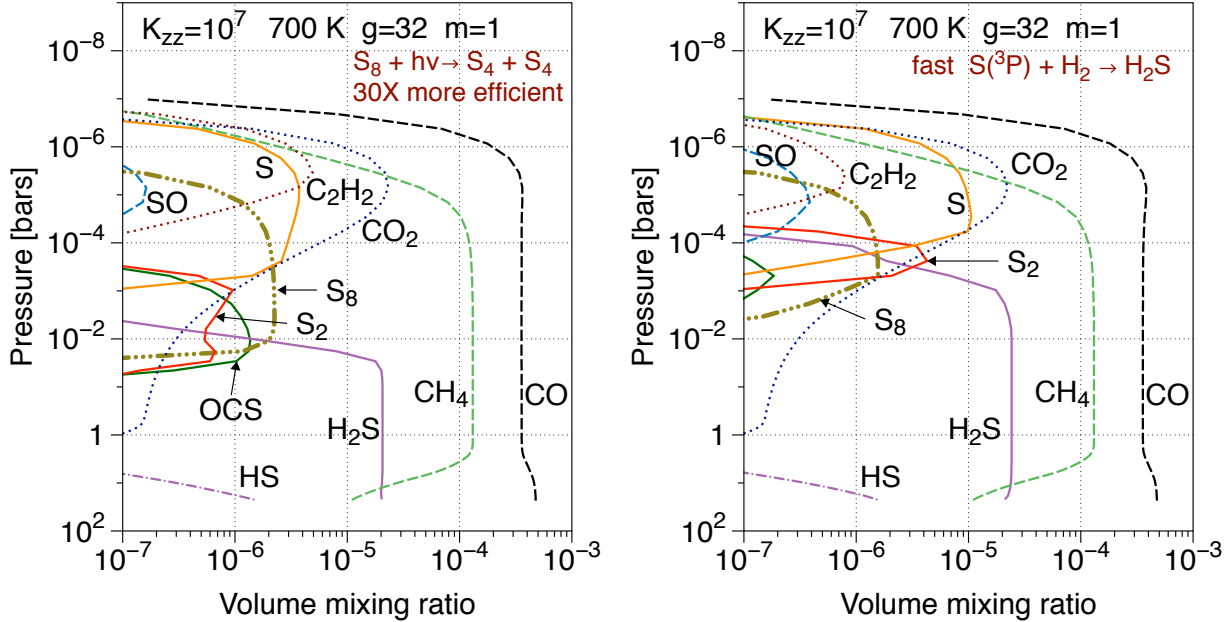
440 yield is reduced.

Fig. 9.— Two sensitivity tests to compare to Figure 1. *Left.* Enhancing the efficiency of S_8 photolysis at low pressures by raising N_c in Eq 6 also generates more S-bearing free radicals that reduce the yield of C_2H_2 and other NMHCs at the top of the atmosphere. *Right.* This model uses the faster rate k'_{22r} for the spin-forbidden insertion reaction $H_2 + S(^3P) + M \rightarrow H_2S + M$. The model is quite sensitive to this. With the faster rate H_2S survives to much higher altitudes than in the nominal model (Figure 1) and S_8 is less abundant and restricted to higher levels in the atmosphere. Photolysis of other sulfur-containing small molecules generates S-bearing free radicals that reduce the yield of C_2H_2 and other NMHCs.

5.3.   Sensitivity to H_2S recombination

442 Rates of many of the chemical reactions that involve sulfur are poorly known. In particular,
443 a major source of model pathology is the 3-body recombination of H_2S, either from HS and H,
444 or from H_2 and S. There is limited information on H_2S recombination, but the reverse process,
445 thermolysis of H_2S, is industrially important and has been the subject of several experiments that
446 elude easy consensus (Bowman and Dodge 1977; Roth et al. 1982; Tesner et al. 1990; Woiki and
447 Roth 1994, 1995a; Olschewski et al. 1994; Shiina et al. 1996, 1998; Karan et al. 1999). Measured
448 rates from high temperature ($1800 < T < 3500$ K) shock tube experiments in Ar (Bowman and
449 Dodge 1977; Woiki and Roth 1994, 1995a; Olschewski et al. 1994; Shiina et al. 1996, 1998) differ
450 among themselves by an order of magnitude; it is not clear why. Moreover, lower temperature
451 ($800 < T < 1400$ K) flow reactor experiments in N_2 (Tesner et al. 1990; Karan et al. 1999) imply
452 rates that are 100-300 times higher than extrapolation of the shock tube data predict.

It was at first presumed that the dominant decomposition channel was

$$H_2S + M \rightarrow HS + H + M \tag{R21}$$

as with H_2O, because the alternative

$$H_2S + M \rightarrow H_2 + S(^3P) + M, \tag{R22}$$

although much less endothermic, is spin forbidden (Roth et al. 1982). But parallel shock tube experiments by Woiki and Roth (1994), who monitored $S(^3P)$ production, and Olschewski et al. (1994), who monitored H_2S disappearance, gave a consistent picture of the spin-forbidden path being dominant. The straightforward, thermodynamically self-consistent reverse reaction

$$H_2 + S(^3P) + M \rightarrow H_2S + M \tag{R22r}$$

was therefore predicted to be fast at low temperatures. The possibility that the interesting reaction R22r might be fast motivated follow-up experiments by Woiki and Roth (1995a) and Shiina et al. (1996, 1998) to directly determine the reaction rate between $S(^3P)$ and H_2. Shiina et al. (1998) found that, for $T > 900$ K, R22r is negligible compared to the competing abstraction reaction

$$H_2 + S(^3P) \rightarrow HS + H. \tag{R9r}$$

Shiina et al. (1998) do not dispute that R22 is the more important thermolysis channel for H_2S, but they change the extrapolation to low temperatures to take into account the considerable energy barrier that they computed,

$$k_{22} = 8.9 \times 10^{-7} \, (T/300)^{-2.61} \exp\left(-44640/T\right). \tag{7}$$

The rate we use for R22r in our standard models is the reverse of k_{22},

$$k_{22r} = 1.4 \times 10^{-31} \, (T/300)^{-1.9} \exp\left(-8140/T\right), \tag{8}$$

which is far below the upper bound determined by Shiina et al. (1998) and very slow (but not negligible) at low temperatures.

For the sensitivity test (Figure 9, right-hand panel) we use a parallel pair of rates that are consistent both with the higher thermolysis rates reported by Olschewski et al. (1994) and Woiki and Roth (1994) and with the lower activation energy estimated by Olschewski et al. (1994):

$$k'_{22} = 8.9 \times 10^{-7} \, (T/300)^{-2.61} \exp\left(-38800/T\right) \tag{9}$$

with reverse

$$k'_{22r} = 1.4 \times 10^{-31} \, (T/300)^{-1.9} \exp\left(-2300/T\right). \tag{10}$$

The rate k'_{22r} is comparable to the upper bound reported by Shiina et al. (1998). Although much slower than the rate that Shiina et al. (1998) had hoped to see, k'_{22r} is fast enough to affect our

475 results significantly (Figure 9). With k'_{22r}, H_2S reaches altitudes 3 scale heights above where it gets
476 to with k_{22r}.

477   We do not attempt to take into account the flow reactor data. These experiments suggest
478 thermolysis rates that are orders of magnitude faster than either k_{22} or k'_{22} at 1000 K, and therefore
479 the recombination reactions must also be. However, we were unable to reproduce Karan et al.
480 (1999)'s argument that the different reported rates can be brought into agreement. We favor the
481 shock tube data because the flow reactor system is more complicated (more reactions need to be
482 taken into account) and less straightforwardly interpreted. E.g., what Karan et al. (1999) actually
483 measured is whether the system has had time enough to reach thermochemical equilibrium, which
484 isn't quite the same thing as determining a particular reaction rate. In the end, we think that the
485 slower rates k_{22r} and k'_{22r} are more plausible given the extensive molecular rearrangements that
486 must occur if an unlikely-looking reaction like R22r is to take place

5.4. Sensitivity to S_n polymerization

488   Our nominal sulfur polymerization scheme is mostly encompassed by reactions R2-R8 in Table
489 1. We have kept the system simple because the reactions and rates are very uncertain. Our rates are
490 similar to those used elsewhere (e.g., Moses et al. 2002; Yung et al. 2009) and are not inconsistent
491 with the few experimental reports (Fair and Thrush 1969; Langford and Oldershaw 1972, 1973;
492 Nicholas et al. 1979). For the sensitivity tests we raise [lower] the rates of

$$S + S_3 + M \rightarrow S_4 + M \tag{R4}$$

493 and

$$S_2 + S_2 + M \rightarrow S_4 + M \tag{R5}$$
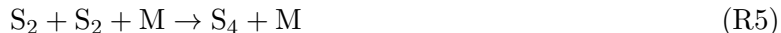
494 by a factor of 10, and raise [lower] the rate of

$$S_4 + S_4 + M \rightarrow S_8 + M \tag{R7}$$

495 by a factor of 100. These two cases of faster and slower polymerization are illustrated in left- and
496 right-hand panels of Figure 10, respectively. The figure shows that our model is not very sensitive
497 to reasonable uncertainties in the sulfur polymerization rate.

5.5. Sensitivity to unknown mechanisms of S_8 chemical destruction

499   Other than photolysis, the main sink of S_8 in our basic model is thermal destruction

$$S_8 + M \rightarrow S_4 + S_4 + M. \tag{R7r}$$

500 This is predicted to be rather fast, because ΔH is a relatively modest 150 kJ/mol, there is a
501 considerable gain in entropy, and the rate for the forward reaction R7 is probably fast. We know of
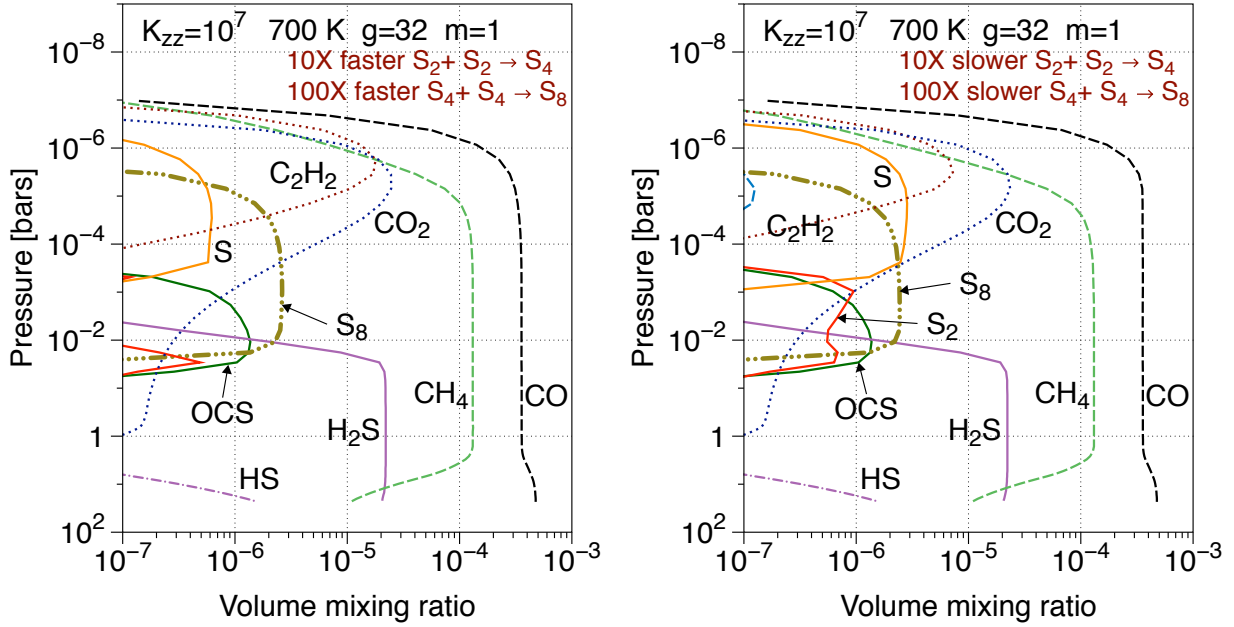
Fig. 10.— Sensitivity of results to rates of S_n polymerization (to be compared to Figure 1). *Left.* Faster polymerization decreases the abundances of S and S_2 without noticeably changing S_8, because in the nominal case most of the sulfur was already pooling in S_8. *Right.* Slower polymerization increases the abundances of S and S_2, but not enough in this model to noticeably affect the S_8 abundance. The greater abundance of S-bearing radicals causes the acetylene (C_2H_2) yield to shrink.

no reported kinetic data regarding S_8's reactions. Yet S_8 should be reactive because reactions with important free radicals should be significantly exothermic. To test the sensitivity of our model to these unknown reactions, we need to invent both the reactions and the products. The most abundant free radical by far is H, which makes reactions with H the likeliest to be important.

At high pressures we might expect a 3-body reaction to unmake the ring into a quasi-linear HS_8 radical, which would then be followed by reactions that either return S_8 or cleave the S_8 chain. We have not pursued this strategy here because (i) we would have to invent many species and many rates and (ii) our rate for R7r is pretty fast at high pressures.

At low pressures any plausible reaction would have to cleave the chain in two places. The invented reaction that adds the least new complexity to our model is

$$S_8 + H \rightarrow HS_4 + S_4, \tag{R51}$$

because we need to add only one invented species, HS_4. We estimate a standard heat of formation of 110 kJ/mol and standard entropy of 330 J/mol/K by analogy to HS_2 (Benson 1978). The invented reaction R51 is therefore substantially exothermic but undoubtedly faces a considerable energy barrier. We consider a slow rate

$$k_{\text{slow}} = 3 \times 10^{-12} \exp\left(-5000/T\right) \tag{11}$$

516 and a fast rate

$$k_{\mathrm{fast}} = 1 \times 10^{-11} \exp\left(-2500/T\right). \tag{12}$$

517 For the temperature dependence we use Pauling's rule of thumb (Pauling 1970, p. 568) that the
518 activation barrier of a radical-molecule reaction is about 8% of the bond energy of the bond to be
519 broken. The slow rate presumes that the two S-S bonds are additive.

520 We then need a set of reactions for HS_4. One category of reaction will be the H-abstraction
521 reactions with H, OH, and some other radicals, such as

$$H + HS_4 \rightarrow H_2 + S_4. \tag{13}$$
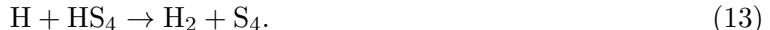
522 These will probably have small activation barriers. At high altitudes S_4 will be promptly photolysed
523 by visible light, so that the sulfur chain is quickly broken down. The other representative category
524 will be molecular rearrangements that reconstitute H_2S, such as

$$H + HS_4 \rightarrow H_2S + S_3. \tag{14}$$

525 Reactions of this type face considerable activation barriers but can be important at depths where
526 downwelling S_8 is converted back to H_2S. For these we use the same 2500 K activation barrier that
527 we used for breaking the S-S bond.

528 Our expectation had been that deep thermal recycling of S_8 would be much sped up by the
529 new chemistry, but this is not really evident in Figure 11. Rather, the greater impact of the new
530 chemistry is to convert S_8 in the upper atmosphere into other more active species, and finally to
531 atomize it. The more abundant S-containing radicals catalyze the oxidation of organics. On the
532 other hand our chemical schemes do not encompass the speculative possibility that sulfur might also
533 catalyze carbon polymerization. In summary, what we don't know about sulfur chemistry appears
534 to have relatively little impact on whether S_8 forms, but there appears to be a strong impact on
535 carbon chemistry. If sulfur does not condense, the fast rate k_{fast} for S_8 destruction does not bode
536 well for organic hazes. Prospects for organics then become better in cooler atmospheres because
537 sulfur condensation would deplete S-containing radicals above the cloudtops.

538 ## 6. Discussion

539 Photochemical hazes are widespread in the solar system but they are not yet established as fact
540 on any actual exoplanet. Observations do not go much beyond showing that many exoplanetary
541 spectra require a broad-band opacity resembling that of clouds. What these clouds might be made
542 of has been a problem for theory (Morley et al. 2015), but as many substances can condense, it is
543 reasonable to expect that there are many kinds of cloud.

544 Our purpose when we began this study was to make a case for organic hazes on the particular
545 planet 51 Eri b. The idea was to use C_4H_2, the first product of acetylene polymerization, as a proxy
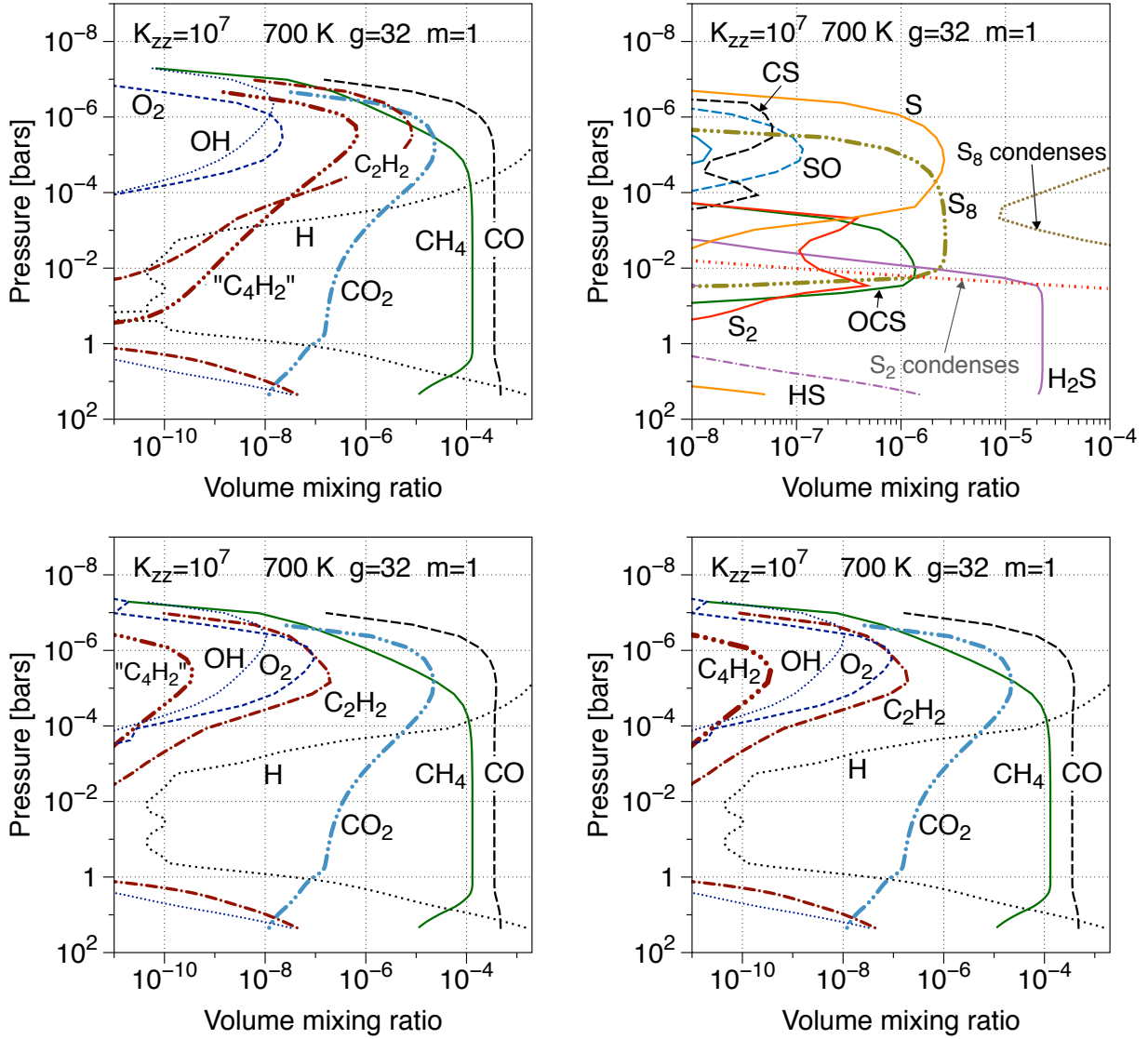
Fig. 11.— Chemical sensitivity tests. *Top.* With the slow rate $k_{\rm slow}$ (Eq 11) for H+S_8, the nominal model is little altered, although there is notably more atomic S at high altitudes. *Bottom.* With the fast rate $k_{\rm fast}$ (Eq 12), the model looks rather different, with S_8 eliminated above 100 μbars and much increased abundances of photochemically active S-containing radicals and molecules. The overall character of the upper atmosphere is more oxidized, acetylene is much reduced, and the proxy "C_4H_2" is nearly wiped out.

for further polymerization: every "C_4H_2" formed was assumed to eventually become incorporated into a particle. The quotes on "C_4H_2" indicate that we are no longer talking about C_4H_2 the molecule but instead about everything downstream from it. But even in those cases where we have clearly tipped the scales to favor "C_4H_2," it only becomes more abundant than C_2H_2 at depths well below the primary photochemical region, where conditions are more reducing. It doesn't help

our case that when we treat C_4H_2 as an actual molecule subject to cracking, we find that there isn't all that much of it there. In summary, the case for soots is intriguing but falls short of being compelling.

On the other hand we have rediscovered the importance of sulfur. Sulfur can have a disproportionate influence on photochemistry because most S-bearing species are relatively easily photolyzed by UV photons with $\lambda > 200$ nm, which 51 Eri a, an F star, emits copiously. Thus sulfur photochemistry becomes a major source of free radicals that can catalyze other chemistries. One consequence of sulfur catalysis is a tendency to drive carbon away from the disequilibrium NMHCs and toward the stronger bonds of CO and CO_2.

More interesting is that sulfur itself can be the photochemical cloud that we are looking for. We find that for a wide range of conditions the major photochemical product of sulfur in a planet like 51 Eri b is the ring molecule S_8, which typically forms at ~ 10 mbars and extends up to 100 μbars. The overall sulfur cycle is simple: H_2S flows up and S_8 and H_2 flow down. In the cooler half of our models sulfur condenses to make a photochemical haze that, depending on particle size, can be optically thick, while in the warmer half of the models sulfur remains in the vapor phase. The sulfur vapor itself might also be optically important, especially at the interface between abyssal H_2S and S_8, where the latter thermally decomposes into a wide range of optically active molecules that are eventually hydrogenated to recombine H_2S. The sulfur photochemistry we have discussed in this paper is quite general and ought to be found in a wide variety of worlds over a broad temperature range, both much cooler and much hotter than the 650-750 K range studied here, and will be present on planets where the UV irradiation is very weak. Sulfur clouds should be found in many of these. Whether 51 Eri b itself is cold enough for sulfur to condense cannot be answered until radiative transfer models incorporate sulfur vapors and sulfur clouds, which is a project beyond the scope of this paper, or until the yellow clouds are seen.

7. Acknowledgements

REFERENCES

Abelson, P. (1966). Chemical events on the primitive Earth. Proc. Natl. Acad. Sci. USA 55, 1365-1372.

Agúndez, M., Venot, O., Iro, N., Selsis, F., Hersant, F., Hébrard, E., Dobrijevic, M., (2012). The impact of atmospheric circulation on the chemistry of the hot Jupiter HD 209458b. Astron. Astrophys. 548, A73.

Agúndez, M., Parmentier, V., Venot, O., Hersant, F., Selsis, F., (2014). Pseudo 2D chemical model of hot-Jupiter atmospheres: application to HD 209458b and HD 189733b. Astron. Astrophys. 564, A73.

Agúndez, M., Venot, O., Selsis, F., Iro, N., (2014). The Puzzling Chemical Composition of GJ 436b's Atmosphere: Influence of Tidal Heating on the Chemistry. Astrophys. J. 781, 781.

Anders, E., Grevasse, N., (1989). Abundances of the elements: Meteoritic and solar. Geochim. Cosmochim. Acta 53, 197-214.

Atkinson, R., Baulch, D.L., Cox, R.A., Crowley, J.N., Hampson, R.F., Hynes, R.G., Jenkin, M.E., Rossi, M.J., Troe, J. (2004), Evaluated kinetic and photochemical data for atmospheric chemistry: Volume I - gas phase reactions of Ox, HOx, NOx and SOx species. *Atmos. Chem. Phys. 4,* 1461-1738.

Benneke, B., (2015). Strict Upper Limits on the Carbon-to-Oxygen Ratios of Eight Hot Jupiters from Self-Consistent Atmospheric Retrieval. ArXiv e-print 1504.07655.

Benson, S.W. (1978). Thermochemistry and kinetics of sulfur-containing molecules and radicals. Chem. Rev. 78, 23-35. DOI: 10.1021/cr60311a003.

Bowman, C.T., Dodge, L.G., (1977). Kinetics of the Thermal Decom- position of Hydrogen Sulfide Behind Shock Waves. 16th Symp. (Int.) Combust. 16, 971.

Darwin, D.C., Moore, C.B. (1995). Reaction rate constants (295 K) for ^{3}CH2 with H2S, SO2, and NO2: upper bounds for rate constants with less reactive partners. J. Phys. Chem. 99, 13467-13470.

DeMore, W.B., Sander, S.P., Golden, D.M., Hampson, R.F., Kurylo, M.J., Howard, C.J., Ravishankara, A.R., Kolb, C.E., Molina, M.J. (1997). Chemical kinetics and photochemical data for use in stratospheric modeling. Evaluation number 12. JPL Publication 97-4.

Du, S.Y., Francisco, J.S., Shepler, B.C., Peterson, K.A. (2008). Determination of the rate constant for sulfur recombination by quasiclassical trajectory calculations. J. Chem. Phys. 128, 204306.

Eiteneer, B., Frenklach, M., (2003). Experimental and Modeling Study of Shock-Tube Oxidation of Acetylene. Int. J. Chem. Kinet. 35, 391-414.

Fair, R.W., Thrush, B.A. (1969). Mechanism of S2 chemiluminescence in the reaction of hydrogen atoms with hydrogen sulphide. Trans. Faraday Soc. 65, 1208-1218.

Freytag, B., Allard, F., Ludwig, H.-G., Homeier, D., Steffen, M. (2010). The role of convection, overshoot, and gravity waves for the transport of dust in M dwarf and brown dwarf atmospheres. Astron. Astrophys. 513, A19 (14 pp.).

Griffith, C.A., Yelle, R.V., Marley, M.S. (1998). The Dusty Atmosphere of the Brown Dwarf Gliese 229B. Science 282, 2063-2065.

Hansen, N., Klippenstein, S.J., Taatjes, C.A., Miller, J.A., Wang, J., Cool, T.A., Yang, B., Yang, R., Wei, L., Huang, C., Wang, J., Qi, F., Law, M.E., Westmoreland, P.R., (2006). Identification and Chemistry of C4H3 and C4H5 Isomers in Fuel-Rich Flames. J. Phys. Chem. A, 110, 3670-3678.

Harding, L.B., Klippenstein, S.J., Georgievskii, Y., (2007). On the combination reactions of hydrogen atoms with resonance-stabilized hydrocarbon radicals. J. Phys. Chem. A 111, 3789-3801.

Harrington, J, de Pater, I., Brecht, S.H., Deming, D., Meadows, V., Zahnle, K.J., Nicholson, P. (2004). Lessons from Shoemaker-Levy 9 about Jupiter and Planetary Impacts. In Jupiter: The Planet, Satellites and Magnetosphere, F. Bagenol, T. Dowling, W. McKinnon, eds. Cambridge Univ. Press. pp. 158-184.

Hills, A.J., Cicerone, R.J., Calvert, J.G., Birks, J.W. (1987). Kinetics of the reactions of S2 with O, O2, O3, N2O, NO, and NO2. J. Phys. Chem. 91, 1199-1204.

Hu, R., Seager, S., (2014). Photochemistry in Terrestrial Exoplanet Atmospheres. III. Photochemistry and Thermochemistry in Thick Atmospheres on Super Earths and Mini Neptunes. Astrophys. J. 784, 63.

Hubeny, I., Burrows, A. (2007). A systematic study of departures from chemical equilibrium in the atmospheres of substellar mass objects. Astrophys. J. 669, 1248-1261.

Karan, K., Mehrotra, A.K., Leo A. Behie, L.A., (1999). On reaction kinetics for the thermal decomposition of hydrogen sulfide. Amer. Inst. Chem. Eng. J. 45, 383-389.

Kasting, J.F., Zahnle, K.J., Pinto, J., Young, A. (1989). Sulfur, ultraviolet radiation, and the early evolution of life. Origins of Life 19, 95-108.

Klippenstein, S.J., Miller, J.A., (2005). The addition of hydrogen atoms to diacetylene and the heats of formation of i-C4H3 and n-C4H3. J. Phys. Chem. A 109, 4285-4295.

Kopparapu, R.K., Kasting, J.F., Zahnle, K.J., (2012)Kopparapu, R. k. and Kasting, J. F. and Zahnle, K. J., A Photochemical Model for the Carbon-rich Planet WASP-12b. Astrophys. J. 745, 77.

Koskinen, T.T., Harris, M.J., Yelle, R.V., Lavvas, P., (2013). The escape of heavy atoms from the ionosphere of HD 209458b. I. A photochemical-dynamical model of the thermosphere. Icarus 226, 1678-1694.

Kurbanov, M.A., Mamedov, Kh.F. (1995). The role of the reaction CO + SH → COS + H in hydrogen formation in the course of interaction between CO and H2S. Kinet. Catal. 36, 455-457.

Langford, R.B., Oldershaw, G.A., (1973). Mechanism of Sulfur Formation in the Flash Photolysis of Carbonyl Sulphide. J. Chem. Soc. Faraday Trans. 69, 1389.

Langford, R.B., Oldershaw, G.A., (1972). Flash Photolysis of H_2S. J. Chem. Soc. Faraday Trans. 68, 1550.

Lavvas, P., Koskinen, T., Yelle, R.V., (2014). Electron Densities and Alkali Atoms in Exoplanet Atmospheres. Astrophys. J. 796, (15 pp).

Lee, J.H., Stief, L.J., Timmons, R.B. (1977). Absolute Rate Parameters for the Reaction of Atomic Hydrogen with Carbonyl Sulfide and Ethylene Episulfide, J. Chem. Phys. 67, 1705-1714.

Liang, M.C., Parkinson, C.D., Lee, A.Y.-T., Yung, Y.L., Seager, S. (2003). Source of atomic hydrogen in the atmosphere of HD 209458b. Astrophys. J. 596, L247-L250.

Liang, M.C., Seager, S., Parkinson, C.D., Lee, A.Y.-T., Yung, Y.L. (2003). On the Insignificance of Photochemical Hydrocarbon Aerosols in the Atmospheres of Close-in Extrasolar Giant Planets Astrophys. J. 605, L61-L64.

Line, M.R., Liang, M.-C., Yung, Y.L. (2010). High-Temperature Photochemistry in the Atmosphere of HD 189733b. Astrophys. J. 717, 496-502.

Line, M.R., Vasisht, G., Chen, P., Angerhausen, D., Yung, Y.L. (2011). Thermochemical and Photochemical Kinetics in Cooler Hydrogen-dominated Extrasolar Planets: A Methane-poor GJ436b? Astrophys. J. 738, article id. 32, 14 pp.

Lodders, K., Fegley, B., (2006). In Chemistry of Low Mass Substellar Objects. Ed. J.W. Mason (Berlin: Springer), pp. 1-31.

Lu, C.W., Wu, Y.J., Lee, Y.P., Zhu, R.S., Lin, M.C. (2004). Experimental and theoretical investigations of rate coefficients of the reaction $S(^3P)$ + O2 in the temperature range 298-878 K. J. Chem. Phys. 121, 8271-8278

Lu, C.W.,Wu, Y.J.,Lee, Y.P.,Zhu, R.S.,Lin, M.C. (2006). Experimental and theoretical investigation of rate coefficients of the reaction $S(^3P)$ + OCS in the temperature range of 298-985 K. J. Chem. Phys. 125, 164329.

Lyons, J.R. (2008). An estimate of the equilibrium speciation of sulfur vapor over solid sulfur and implications for planetary atmospheres. J. Sulfur Chem. 29, 269-279.

Macintosh, B., Graham, J.R., Barman, T., De Rosa, R.J., Konopacky, Q., Marley, M.S., Marois, C., Nielsen, E.L., Pueyo, L., Rajan, A., and 72 coauthors (2015). Discovery and spectroscopy of the young jovian planet 51 Eri b with the Gemini Planet Imager. Science 350, 64-67.

Marley, M.S., Fortney, J.J., Seager, S., Barman, T. (2007). An Imposing and Comprehensive Title. In Protostars and Planets V. Eds. B. Reipurth, D. Jewitt, and K. Keil. Univ. Ariz. Press, Tucson, pp. 733–747.

Meyer, B., (1976). Elemental sulfur. Chemical Reviews 76, 367-387.

Miguel, Y., Kaltenegger, L., (2014). Exploring Atmospheres of Hot Mini-Neptunes and Extrasolar Giant Planets Orbiting Different Stars with Application to HD 97658b, WASP-12b, CoRoT-2b, XO-1b, and HD 189733b, Astrophys. J. 780, 166.

Miguel, Y., Kaltenegger, L., Linsky, J.L., Rugheimer, S., (2015) The effect of Lyman α radiation on mini-Neptune atmospheres around M stars: application to GJ 436b. Mon. Not. Roy. Astron. Soc. 446, 345-353.

Millar, T.J., Farquhar, P.R.A., Willacy, K., (1997). The UMIST database for astrochemistry 1995. Astron. Astrophys. Suppl. Ser. 121, 139-185.

Miller-Ricci Kempton, E., Zahnle, K., Fortney, J.J. (2011). The Atmospheric Chemistry of GJ 1214b: Photochemistry and Clouds. Astrophys. J. 745, 3 (13pp).

Morley, C.V., Fortney, J.J., Visscher, C., Marley, M.S., Sauman, D., Legett, S.K. (2012). Neglected clouds in T and Y dwarf atmospheres. Astrophys. J. 756, article id. 172, 17 pp.

Morley, C.V., Fortney, J.J., Kempton, E.M.R., Marley, M.S., Visscher, C., Zahnle, K.J. (2013). Quantitatively Assessing the Role of Clouds in the Transmission Spectrum of GJ 1214b. Astrophys. J. 775, article id. 33, 13 pp.

Morley, C.V., Fortney, J.J., Kempton, E.M.R., Marley, M.S., Visscher, C., Zahnle, K.J. (2013). Quantitatively Assessing the Role of Clouds in the Transmission Spectrum of GJ 1214b. Astrophys. J. 775, article id. 33, 13 pp.

Moses, J.I., Nash, D.B., (1991). Phase transformations and the spectral reflectance of solid sulfur: can metastable sulfur aIIotropes exist on Io? Icarus 89, 277-304.

Moses, J.I. Allen, M., Gladstone, G.R. (1995). Post-SL9 sulfur photochemistry on Jupiter. Geophys. Res. Lett. 22, 1597-1600.

Moses, J.I., Zolotov, M.Y., Fegley, B. (2002). Photochemistry of a volcanically driven atmosphere on Io: Sulfur and oxygen species from a Pele-type eruption. Icarus 156, 76-106.

Moses, J.I., Fouchet, F., B'ezard, B., Gladstone, G.R., Lellouch, E., Feuchtgruber, H. (2005). Photochemistry and diffusion in Jupiter's stratosphere: Constraints from ISO observations and comparisons with other giant planets. J. Geophys. Res. 110, E08001 (45 pp.).

Moses, J.I., Visscher, C., Fortney, J.J., Showman, A.P., Lewis, N.K., Griffith, C.A., Klippenstein, S.J., Shabram, M., Friedson, A.J., Marley, M.S., Freedman, R.S. (2011). Disequilibrium

Carbon, Oxygen, and Nitrogen Chemistry in the Atmospheres of HD 189733b and HD 209458b. Astrophys. J. 737, article id. 15, 37 pp.

Moses, J.I., Madhusudhan, N., Visscher, C., Freedman, R.S. (2013). Chemical Consequences of the C/O Ratio on Hot Jupiters: Examples from WASP-12b, CoRoT-2b, XO-1b, and HD 189733b. Astrophys. J. 763, article id. 25, 26 pp.

Moses, J.I., Line, M.R., Visscher, C., Richardson, M.R., Nettelmann, N., Fortney, J.J., Barman, T.S., Stevenson, K.B., Madhusudhan, N. (2013). Compositional Diversity in the Atmospheres of Hot Neptunes, with Application to GJ 436b. Astrophys. J. 777, article id. 34, 23 pp.

Moses, J.I. (2014). Chemical Kinetics on Extrasolar Planets. Phil. Trans. Roy. Soc. A 372, 20130073. DOI: 10.1098/rsta.2013.0073.

Nicholas, J.E., Amodio, C.A., Baker, M.J. (1979). Kinetics and Mechanism of the Decomposition of H_2S, CH_2SH and $(CH_3)_2S$ in a Radio-frequency Pulse Discharge J. Chem. Soc. Faraday Trans. 75, 1868.

Olschewski, H.A., J. Troe, Wagner, H.Gg., (1994). UV absorption study of the thermal decomposition reaction $H_2S \rightarrow H_2 + S(^3P)$. J. Phys. Chem. 98, 12964-12967.

Oya, M., Shiina, H., Tsuchiya, K., Matsui, H. (1994). Thermal decomposition of COS. Bull. Chem. Soc. Japan 67, 2311-2313.

Pauling, L. (1970). General Chemistry. Dover.

Pavlov, A.A., Kasting, J.F., (2002). Astrobiology

Pen, J., Hu, X., Marshall, P. (1999). Experimental and *ab initio* investigations of the kinetics of the reaction of H atoms with H_2S. J. Phys. Chem. A, 103, 5307-5311.

Perrin, D., Richard, C., Martin, R. (1988). Etude cinetique de la reaction thermique du pentene-2 cis vers 500°C. III - Influence de H_2S. J. Chim. Phys. 85, 185-192.

Pinto, J., Gladstone, R., Yung, Y., (1980). Photochemical production of formaldehyde in the Earth's primitive atmosphere. Science 210, 183-185.

Rimmer, P.B., Helling, C., (2016). A Chemical Kinetics Network for Lightning and Life in Planetary Atmospheres. Astrophys. J. Supp., *accepted.* arXiv:1510.07052.

Roth, P., Lohr, R., Braner, U., (1982). Thermal Decomposition of Hydrogen Sulfide at Low Concentrations. Combust. Flame 45, 273.

Sander, S.P., Friedl, R.R., Ravishankara, A.R., Golden, D.M., Kolb, C.E., Kurylo, M.J., Huie, R.E., Orkin, V.L., Molina, M.J., Moortgat, G.K., Finlayson-Pitts, B.J. (2003). Chemical

Kinetics and Photochemical Data for Use in Atmospheric Studies. Evaluation Number 14. JPL Publication 02-25.

Schofield, K. (1973). Evaluated chemical kinetic rate constants for various gas phase reactions. J. Phys. Chem. Ref. Data 2, 25-84.

Shiina, H., Oya, M., Yamashita, K., Miyoshi, A., Matsui, H. (1996). Kinetic studies on the pyrolysis of H_2S. Phys. Chem. 100, 2136-2140.

Shiina, H., Miyoshi, A., Matsui, H. (1998). Investigation on the insertion channel in the $S(^3P)$ + H_2 reaction. J. Phys. Chem. A 102, 3556 - 3559.

Shum, L.G.S., Benson, S.W., (1985). The pyrolysis of dimethyl sulfide, kinetics and mechanism. Int. J. Chem. Kinet. 17, 749.

Singleton, D.L., Cvetanovic, R.J. (1988). Evaluated chemical kinetic data for the reactions of atomic oxygen $O(^3P)$ with sulfur containing compounds. J. Phys. Chem. Ref. Data 17, 1377-1399.

Spencer, J.R., Jessup, K.L., McGrath, M.A., Gilda E. Ballester, G.E., Roger Yelle, R.V. (2000). Discovery of gaseous S_2 in Io's Pele plume. Science 288, 1208-1210.

Tesner, P.A., Nemirovskii, M.S., Motyl, D.N. (1990). Kinetics of the thermal decomposition of hydrogen sulfide at 600-1200°C. Kinet. Catal. 31, 1081-1083.

Tsuchiya, K.,Yamashita, K., Miyoshi, A., Matsui, H. (1996). Studies on the reactions of atomic sulfur (^3P) with H_2, D_2, CH_4, C_2H_6, C_3H_8, n-C_4H_{10}, and i-C_4H_{10}. J. Phys. Chem. 100, 17202-17206.

Tsuchiya, K., Kamiya, K., Matsui, H., (1997). Studies on the Oxidation Mechanism of H_2S Based on Direct Examination of the Key Reaction. Int. J. Chem. Kinet. 29, 57.

Venot, O., Hébrard, E., Agúndez, M., Dobrijevic, M., Selsis, F., Hersant, F., Iro, N., Bounaceur, R., (2012). A chemical model for the atmosphere of hot Jupiters. Astron. Astrophys. 546, A43.

Venot, O., Fray, N., Bénilan, Y., Gazeau, M.-C., Hébrard, E., Larcher, G., Schwell, M., Dobrijevic, M., Selsis, F., (2013). High-temperature measurements of VUV-absorption cross sections of CO_2 and their application to exoplanets. Astron. Astrophys. 551, A131.

Venot, O., Agúndez, M., Selsis, F., Tessenyi, M., Iro, N., (2014). The atmospheric chemistry of the warm Neptune GJ 3470b: Influence of metallicity and temperature on the CH_4/CO ratio. Astron. Astrophys. 562, A51.

Venot, O., Hébrard, E., Agúndez, M., Decin, L., Bounaceur, R., (2015). New chemical scheme for studying carbon-rich exoplanet atmospheres. Astron. Astrophys. 577, A33.

Visscher, C.W., Lodders, K., Fegley, B. (2006). Atmospheric chemistry in giant planets, brown dwarfs, and low-mass dwarf stars. ii. Sulfur and phosphorus. Astrophys. J. 648, 1181-1195.

Visscher, C.W., Moses, J.I. (2011). Quenching of carbon monoxide and methane in the atmospheres of cool brown dwarfs and hot Jupiters. Astrophys. J. 738, article id. 72, 12 pp.

Visscher, C.W. (2012). Chemical timescales in the atmospheres of highly eccentric exoplanets. Astrophys. J. 757, article id. 5, 8 pp.

Vuitton, V., Yelle, R.V., Lavvas, P., Klippenstein, S.J. (2012). Rapid association reactions at low pressure: impact on the formation of hydrocarbons on Titan. Astrophys. J. 744, article id. 11, 7 pp.

Woiki, D.; Roth, P. (1994). Kinetics of the high-temperature H_2S decomposition. J. Phys. Chem. 98, 12958-12963.

Woiki, D., Roth, P., (1995a). A shock tube study of the reaction $S + H_2 = SH + H$ in pyrolysis and photolysis systems. Int. J. Chem. Kinet. 27, 547-553.

Woiki, D., Roth, P. (1995b). Oxidation of S and SO by O_2 in high-temperature pyrolysis and photolysis reaction systems. Int. J. Chem. Kinet. 27, 5-71.

Young A.T. (1983). Venus cloud microphysics. Icarus 56, 568.

Yung, Y.L., Liang, M.C., Jiang, X., Shia, R.L., Lee, C., Bézard B., Marcq, E., (2009). Evidence for carbonyl sulfide (OCS) conversion to CO in the lower atmosphere of Venus. J. Geophys. Res. 114, E00B34.

Zahnle, K.J, Mac Low, M.-M., Lodders, K., B. Fegley, B. (1995). Sulfur chemistry in the wake of Comet Shoemaker-Levy 9. Geophys. Res. Lett. 22, 1593-1596.

Zahnle, K.J., Marley, M.S., Freedman, R.S., Lodders, K., Fortney, J.J. (2009). Atmospheric sulfur chemistry on hot Jupiters. Astrophys. J. Lett. 701, L20-L24.

Zahnle, K.J., Marley, M.S. (2014). Methane, Carbon Monoxide, and Ammonia in Brown Dwarfs and Self-Luminous Giant Planets. Astrophys. J. 797, article id. 41, 19 pp.

Table 1

	Reactants		Products	Rate $[\text{cm}^3\text{s}^{-1}]$ or $[\text{cm}^6\text{s}^{-1}]$	Reference
R1	$S + S + M^*$	$\rightarrow$	$S_2 + M$	$2.0\times10^{-33}e^{206/T}$	Du et al. (2008)
	$S + S$	$\rightarrow$	S_2	$2.3\times10^{-14}e^{415/T}$	Du et al. (2008)
R2	$S + S_2 + M$	$\rightarrow$	$S_3 + M$	$1.0\times10^{-30}\,(T/298)^{-2.0}$	assumed
	$S + S_2$	$\rightarrow$	S_3	5.0×10^{-11}	assumed
R3	$S + S_3$	$\rightarrow$	$S_2 + S_2$	4.0×10^{-11}	assumed
R4	$S + S_3 + M$	$\rightarrow$	$S_4 + M$	$1.0\times10^{-30}\,(T/298)^{-2.00}$	assumed, varied 10$\times$
	$S + S_3$	$\rightarrow$	S_4	5.0×10^{-11}	assumed
R5	$S_2 + S_2 + M$	$\rightarrow$	$S_4 + M$	$1.0\times10^{-30}\,(T/298)^{-2.00}$	varied 10$\times$, see note
	$S_2 + S_2$	$\rightarrow$	S_4	3.0×10^{-11}	assumed
R6	$S + S_4$	$\rightarrow$	$S_2 + S_3$	$4.0\times10^{-11}e^{-500/T}$	Moses et al. (1995)
R7	$S_4 + S_4 + M$	$\rightarrow$	$S_8 + M$	$7.0\times10^{-30}\,(T/298)^{-2.00}$	assumed, varied 100$\times$
	$S_4 + S_4$	$\rightarrow$	S_8	7.0×10^{-11}	assumed
R8	$S + HS$	$\rightarrow$	$S_2 + H$	1.0×10^{-11}	assumed, see note
R9	$H + HS$	$\rightarrow$	$S + H_2$	$3.0\times10^{-11}\,(T/298)^{0.7}$	reverse of R9r
R9r	$S + H_2$	$\rightarrow$	$H + HS$	$5.3\times10^{-10}\,(T/298)^{0.95}\,e^{-9920/T}$	see note
R10	$HS + HS$	$\rightarrow$	$S_2 + H_2$	$1.3\times10^{-11}e^{-20600/T}$	like $2OH \rightarrow H_2 + O_2$
R11	$H + S_3$	$\rightarrow$	$HS + S_2$	$5.0\times10^{-11}e^{-500/T}$	like $H+O_3 \rightarrow OH+O_2$
R12	$H + S_4$	$\rightarrow$	$HS + S_3$	$5.0\times10^{-11}e^{-500/T}$	like $H + S_3$
R13	$O + HS$	$\rightarrow$	$OH + S$	$1.7\times10^{-11}\,(T/298)^{0.67}\,e^{-956/T}$	Schofield (1973)
R14	$HS + OH$	$\rightarrow$	$H_2O + S$	$4.0\times10^{-12}e^{-240/T}$	inspired by R23
R15	$S + CH$	$\rightarrow$	$HS + C$	$1.7\times10^{-11}\,(T/298)^{0.50}\,e^{-4000/T}$	Millar et al. (1997)
R16	$S + NH$	$\rightarrow$	$HS + N$	$1.7\times10^{-11}\,(T/298)^{0.50}\,e^{-4000/T}$	Millar et al. (1997)
R17	$NH_2 + HS$	$\rightarrow$	$NH_3 + S$	$5.0\times10^{-12}e^{-500/T}$	Moses et al. (1995)
R18	$HS + CH_2$	$\rightarrow$	$S + CH_3$	$4.0\times10^{-12}e^{-500/T}$	Moses et al. (1995)
R19	$HS + CH_3$	$\rightarrow$	$S+ CH_4$	$4.0\times10^{-11}e^{-500/T}$	Shum & Benson (1985)
R20	$S + HCO$	$\rightarrow$	$HS + CO$	6.0×10^{-11}	Moses et al. (1995)
R21	$H + HS + M$	$\rightarrow$	$H_2S + M$	$1.4\times10^{-31}\,(T/298)^{-2.5}\,e^{+500/T}$	see note
	$H + HS$	$\rightarrow$	H_2S	1.0×10^{-10}	assumed
R22	$S + H_2 + M$	$\rightarrow$	$H_2S + M$	$1.4\times10^{-31}\,(T/298)^{-1.9}\,e^{-8140/T}$	see text
	$S + H_2 + M$	$\rightarrow$	$H_2S + M$	$1.4\times10^{-31}\,(T/298)^{-1.9}\,e^{-2300/T}$	alternate rate, see text
	$S + H_2$	$\rightarrow$	H_2S	1.0×10^{-11}	assumed
R23	$H + H_2S$	$\rightarrow$	$HS + H_2$	$3.7\times10^{-12}\,(T/298)^{1.94}\,e^{-455/T}$	Pen et al. (1999)
R24	$H_2S + S$	$\rightarrow$	$HS + HS$	$1.4\times10^{-10}e^{-3720/T}$	Shiina et al. (1996)
R25	$O+ H_2S$	$\rightarrow$	$HS+ OH$	$9.2\times10^{-12}e^{-1800/T}$	DeMore et al. (1997)
R26	$OH + H_2S$	$\rightarrow$	$H_2O + HS$	$6.1\times10^{-12}e^{-81/T}$	Atkinson et al. (2004)
R27	$HS + HCO$	$\rightarrow$	$H_2S + CO$	5.0×10^{-11}	like R20
R28	$CH_2 + H_2S$	$\rightarrow$	$CH_3 + HS$	$2.5\times10^{-11}e^{-750/T}$	Darwin&Moore (1995)
R29	$H_2S + CH_3$	$\rightarrow$	$HS + CH_4$	$2.1\times10^{-13}e^{-1160/T}$	Perrin et al. (1988)
R30	$O + HS$	$\rightarrow$	$SO + H$	7.0×10^{-11}	Sander et al. (2003)
R31	$S + OH$	$\rightarrow$	$H + SO$	6.6×10^{-11}	DeMore et al. (1997)
R32	$O + S_2$	$\rightarrow$	$SO + S$	1.1×10^{-11}	Hills et al. (1987)
R33	$S+ O_2$	$\rightarrow$	$SO + O$	$1.5\times10^{-13}\,(T/298)^{2.11}\,e^{-730/T}$	Lu et al. (2004)
R34	$S_3+ O$	$\rightarrow$	$S_2 + SO$	$2.0\times10^{-11}e^{-500/T}$	Moses et al. (1995)

	Reactants		Products	Rate [cm^{3}s^{-1}] or [cm^{6}s^{-1}]	Reference
R35	S$_4$ + O	→	S$_3$ + SO	$2.0\times10^{-11}e^{-500/T}$	Moses et al. (1995)
R36	S + CO +M	→	OCS + M	$3.6\times10^{-34}\,(T/298)^{-0.57}$	see note
	S + CO	→	OCS	3.0×10^{-14}	see note
R37	O + OCS	→	CO + SO	$7.8\times10^{-11}e^{-2620/T}$	Singleton and Cvetanovic (1988)
R38	HS + CO	→	OCS + H	$4.2\times10^{-14}e^{-7660/T}$	Kurbanov et al. (1995)
R39	OCS + S	→	CO + S$_2$	$1.5\times10^{-13}\,(T/298)^{2.57}\,e^{-1180/T}$	Lu et al. (2006)
R40	O + OCS	→	S + CO$_2$	$8.3\times10^{-11}e^{-5530/T}$	Singleton and Cvetanovic (1988)
R41	OCS + OH	→	CO$_2$ + HS	$1.1\times10^{-13}e^{-1200/T}$	Atkinson et al. (2004)
R42	S + HCO	→	OCS + H	6.0×10^{-11}	Moses et al. (1995)
R43	CO + S$_3$	→	S$_2$ + OCS	$1.0\times10^{-11}e^{-10000/T}$	see note
R44	O + CS	→	CO + S	$2.7\times10^{-10}e^{-760/T}$	Atkinson et al. (2004)
R45	S + CH	→	CS + H	2.0×10^{-11}	assumed
R46	OH + CS	→	OCS + H	2.0×10^{-13}	assumed
R47	CH$_2$ + S	→	CS + H$_2$	2.0×10^{-11}	assumed
R48	H + S$_4$ + M	→	HS$_4$ + M	7.0×10^{-30}	assumed
	H + S$_4$	→	HS$_4$	7.0×10^{-11}	assumed
R49	H + S$_8$	→	HS$_4$ + S$_4$	$3.0\times10^{-12}e^{-5000/T}$	assumed, see text
	H + S$_8$	→	HS$_4$ + S$_4$	$3.0\times10^{-11}e^{-2500/T}$	alternate rate
R50	H + HS$_4$	→	H$_2$ + S$_4$	$1.0\times10^{-10}e^{-500/T}$	assumed, see text
R51	H + HS$_4$	→	H$_2$S + S$_3$	$1.0\times10^{-10}e^{-2500/T}$	assumed, see text
R52	OH + HS$_4$	→	H$_2$O + S$_4$	$3.0\times10^{-11}e^{-500/T}$	assumed, see text
R53	NH$_2$ + HS$_4$	→	NH$_3$ + S$_4$	$3.0\times10^{-11}e^{-500/T}$	assumed, see text
R54	HS + HS$_4$	→	H$_2$S + S$_4$	$3.0\times10^{-11}e^{-2500/T}$	assumed, see text
R55	HS$_4$ + HS$_4$	→	H$_2$ + S$_8$	$3.0\times10^{-12}e^{-2500/T}$	assumed, see text
R56	S + HS$_4$	→	HS + S$_4$	$3.0\times10^{-11}e^{-1000/T}$	assumed, see text
R57	C$_2$H + C$_2$H$_2$	→	C$_4$H$_2$ + H	$1.25\times10^{-10}\,(T/298)^{0.24}\,e^{37.3/T}$	Eiteneer&Frenklach(2003)
R58	C$_4$H$_2$ + H + M	→	C$_4$H$_3$ + M	$5.9\times10^{-25}\,(T/298)^{-8.9}\,e^{-1260/T}$	Klippenstein&Miller(2005)
	C$_4$H$_2$ + H + M	→	C$_4$H$_3$ + M	$5.2\times10^{-11}\,(T/298)^{1.2}\,e^{-882/T}$	Klippenstein&Miller(2005)
R59	C$_4$H$_3$ + H	→	C$_4$H$_2$ + H$_2$	$5\times10^{-11}e^{-500/T}$	see text
R60	C$_4$H$_3$ + H	→	C$_2$H$_2$ + C$_2$H$_2$	$5\times10^{-11}e^{-2000/T}$	see text
R61	C$_4$H$_3$ + H	→	C$_4$H$_4$	1.8×10^{-10}	Harding et al. (2007)

* M refers to the background atmosphere, principally H$_2$ and He; units of density [cm^{-3}].

R2-R8. These assumed rates are generally consistent with those of Moses et al. (2002); Yung et al. (2009).

R5. Reported rates are 1×10^{-29} (Langford and Oldershaw 1973), 2.2×10^{-29} (Nicholas et al. 1979).

R8. Reported rates are 4×10^{-11} (Schofield 1973), $<5\times10^{-12}$ (Nicholas et al. 1979).

R9r. A blend of Woiki and Roth (1995a) and Shiina et al. (1998).

R21. This is the reverse of Shiina et al. (1998) upper bound on H$_2$S + M → H + HS + M.

R36. These are reverses of Oya et al. (1994) rate for OCS + M → CO + S + M and of Schofield (1973) high pressure limit OCS → CO + S.

R43. Exothermic, but the analogous CO + O$_3$ → CO$_2$ + O$_2$ has an upper limit at 298 K of 4×10^{-25}.

R45-R47. There is little information re reactions of CS.

R48-R61. HS$_4$ and C$_4$H$_3$ are invoked to create sinks on S$_8$ and C$_4$H$_2$, respectively.